Functional Role for Cas Cytoplasmic Adaptor Proteins During Cortical Axon Pathfinding

Running title: Cas adaptor proteins are required for cortical tract pathfinding

Jason A. Estep [1, *], Alyssa M. Treptow [1, *], Payton A. DePalma [2], Patrick Williamson [3], Wenny Wong [3], Martin M. Riccomagno [1, 2, 3, #]

1 Cell, Molecular and Developmental Biology Graduate Program,

2 Neuroscience Graduate Program,

3 Neuroscience Undergraduate Program, Department of Molecular, Cell & Systems Biology, University of California, Riverside, CA, USA

* These authors contributed equally to this work

Corresponding Author: Martin M. Riccomagno, martinmr@ucr.edu.

Abstract

Proper neural circuit organization requires individual neurons to project to their targets with high specificity. While several guidance molecules have been shown to mediate axonal fasciculation and pathfinding, less is understood about how neurons intracellularly interpret and integrate these cues. Here we provide genetic evidence that the Crk-Associated Substrate (Cas) family of intracellular adaptor proteins is required for proper fasciculation and guidance of two cortical white matter tracts: the Anterior Commissure (AC) and thalamocortical axons (TCAs). Using a *Cas* Triple Conditional Knock Out (*Cas TcKO*) mouse model, we show that Cas proteins are required non-neuronally for TCA projections in a manner that phenocopies the non-neuronal requirement for the β1-integrin receptor. Additional analysis of *Cas TcKO* mutants reveals a neuronal-autonomous role in AC fasciculation that is not phenocopied in β1-integrin deficient mutants, suggesting that Cas proteins might signal downstream of a different receptor during this axon pathfinding event. These findings implicate Cas proteins as key mediators of cortical axon tract fasciculation and guidance.

Introduction

During Central Nervous System (CNS) development, axons often traverse complex routes to meet their synaptic targets, interacting with a diverse array of attractive, repulsive, and permissive cues (Tessier-Lavigne and Goodman 1996; Kolodkin and Tessier-Lavigne 2011). One developmental mechanism proposed to ensure proper guidance of large tracts is the concept of "pioneer" vs "follower" axons (Caudy and Bentley 1986; Lefcort and Bentley 1987; Easter et al. 1993, 1994; Wang and Marquardt 2013). In this framework, initial pioneering axons carve out stereotyped trajectories due to the presence of intermediate targets, or guidepost cells (Chédotal and Richards 2010). These pioneer axons then serve as tracks that subsequent follower axons may use to reach a common target. Both the guidepost-to-guidepost advancement of pioneering axons as well as the regulated fasciculation and defasciculation of follower axons require neurons to properly sense and respond to adhesive signals (Moreland and Poulain 2022; Breau and Trembleau 2023) in the forms of cell-cell and cell-extracellular matrix (ECM) interactions. In the vertebrate nervous system, two well-established examples of guidepost-assisted axonal guidance are thalamocortical axon (TCA) projections (López-Bendito et al. 2006; Garel and López-Bendito 2014) and the commissural tracts of the forebrain such as the Anterior Commissure (AC) (Squarzoni et al. 2015). However, the exact cellular and molecular mechanisms that permit the timely interpretation of adhesive signals during TCA guidance or AC formation remain to be elucidated.

During normal development, TCA projections are guided by a diverse array of secreted gradients, guidepost populations, and intermediate targets as they navigate their way from the thalamus to the developing neocortex (Vanderhaeghen and Polleux 2004; Molnár et al. 2012;

López-Bendito 2018). In mice, TCAs, originating from the thalamus at embryonic day 12 (E12), first turn dorsolaterally at the diencephalic–telencephalic boundary (DTB), then fasciculate to form the internal capsule on E13 and advance through the subpallium until they reach the pallial-subpallial boundary (PSPB) at E14 (Garel and López-Bendito 2014; Molnár and Kwan 2024). At the PSPB, TCAs encounter corticofugal axons and arrest for two to three days before entering the cortical plate, temporarily targeting a cortical region known as the subplate (Ghosh et al. 1990; Allendoerfer and Shatz 1994; Ayoub and Kostovic 2009). Entry of thalamic axons into the cortical layers and coordinated target selection is facilitated by the subplate, a developmentally transient population of the earliest-born telencephalic neurons that serves as an intermediate target for TCA pathfinding (McConnell et al. 1989; Ghosh et al. 1990; Ghosh and Shatz 1992; Allendoerfer and Shatz 1994; Kanold and Luhmann 2010). By E18, TCAs innervate the cortical plate through the intermediate zone and defasciculate to reach their individual targets (Molnár et al. 2012; Garel and López-Bendito 2014), arriving at the neocortex before their target layer (layer IV) is fully formed. Recent studies suggest that TCAs help promote the specification of layer IV neurons as the cortex develops (Monko et al. 2022).

The formation of commissural tracts in the forebrain is also known to involve the assistance of additional intermediate targets, often in the form of transient midline glial populations (Silver et al. 1993; Marcus et al. 1995; Shu and Richards 2001; Shu et al. 2003), such as the glial “tunnel” that facilitates the formation of the Anterior Commissure (Pires-Neto et al. 1998; Lent et al. 2005). The AC is composed of two tracts that share a midline crossing point. Beginning at E14-E15 in mice, axons of the anterior AC (aAC) originate from the Anterior Olfactory Nucleus and form reciprocal connections to each olfactory bulb, while axons of the

79 posterior AC (pAC) originate from the ventrolateral cortex and join with the stria terminalis to
80 form reciprocal connections between the two hemispheres (Jouandet and Hartenstein 1983;
81 Fenlon et al. 2021). Recent developmental studies have identified a population of pioneering
82 axons that precede primary fascicle formation and midline crossing during pAC establishment
83 and suggest a role for ECM molecules in the sorting of aAC and pAC axons (Martin-Lopez et al.
84 2018).

85 The Crk-Associated Substrate (Cas) family of signal adaptor proteins is comprised of four
86 paralogues: p130Cas (Bcar1), Cas-L (HEF1, NEDD9), Sin (EFS), and Cass4 (Defilippi et al. 2006;
87 Deneka et al. 2015). All four Cas paralogues have high sequence conservation and structure
88 similarity with an N-terminal SH3-domain, a central substrate domain containing 15 repeats of
89 the Tyr-X-X-Pro (YxxP) motif, and a serine-rich domain (Deneka et al. 2015). Upon upstream
90 receptor activation, Cas proteins are phosphorylated on tyrosine residues within the substrate
91 domain, thus permitting docking of SH2- and PTB-containing partners such as Crk, CrkL, Nck,
92 and SHIPTP2 (Bouton et al. 2001; Ruest et al. 2001; Fonseca et al. 2004; Defilippi et al. 2006;
93 Donato et al. 2010). Biochemical studies have demonstrated that Cas proteins are
94 phosphorylated downstream of Integrin (Bargon et al. 2005; Huang et al. 2007; Riccomagno et
95 al. 2014), Dystroglycan (Wong et al. 2023), CXCL12/CXCR4 (Wang et al. 2000), Neuropilin (Evans
96 et al. 2011), and Netrin (Liu et al. 2007) signaling. Phosphorylation of Cas induces the assembly
97 of the Cas-Crk-DOCK180 scaffold complex which subsequently recruits and activates Rac
98 GTPases, leading to local actin polymerization (Honda et al. 1999; Gustavsson et al. 2004;
99 Defilippi et al. 2006). In this way, Cas proteins act as an essential link between external adhesion

100 signals and the actin cytoskeleton, permitting cells to reorganize their actin network in response
101 to ECM engagement.

102 Developmentally, Cas proteins have been shown to regulate motor axon fasciculation
103 and projection in Drosophila (Huang et al. 2007), with similar roles in the fasciculation and
104 pathfinding of Dorsal Root Ganglion (DRG) axons in the mammalian Peripheral Nervous System
105 (PNS) (Vahedi-Hunter et al. 2018). In the mammalian CNS, Cas proteins play additional roles
106 during neuronal migration and axonal guidance events: Cas adaptor proteins coordinate
107 commissural projections in the spinal cord (Liu et al. 2007), organize Retinal Ganglion Cell
108 positioning in the mouse retina (Riccomagno et al. 2014), and have been recently shown to
109 participate in cortical lamination (Wong et al. 2023).

110 In this study, we sought to investigate the potential roles of Cas proteins during the
111 formation of forebrain white matter tracts. Using conditional reverse genetics, we have found
112 that Cas proteins are required for proper guidance of TCA projections and fasciculation of pAC
113 axons. We demonstrate that the TCA projection phenotype is cortical-autonomous but non-
114 neuronal-autonomous, with mis-projecting TCA processes closely associating with misplaced
115 subplate and deep layer neurons. Further, we demonstrate a cortical- and neuronal-
116 autonomous role for *Cas* genes during AC fasciculation and show that defasciculating AC axons
117 originate, in part, from the dorsolateral cortex. Interestingly, defects in AC fasciculation are not
118 phenocopied by β1-integrin mutants, suggesting that Cas proteins act, at least in part,
119 independently of β1-integrin during AC formation.

120 **Results**

121 To investigate the potential roles of *Cas* family genes during cortical white matter tract
122 formation, we began by assessing the expression of the *Cas* family paralogues during cortical
123 development. We recently established that transcripts for the paralogues *p130Cas*, *CasL/Nedd9*,
124 and *Sin/Efs* are all expressed in the developing cortex, with overlapping expression in the
125 subventricular and ventricular zones (Wong et al. 2023). The *p130Cas* transcript is dynamically
126 enriched in the cortical plate at E12.5 and the intermediate zone at E14.5, consistent with
127 expression in postmitotic neurons that are projecting axons (Wong et al. 2023). To better
128 visualize axons originating from neurons expressing *p130Cas*, we took advantage of the
129 *p130Cas-EGFP-BAC* transgenic line generated by the GENSAT BAC transgenic project (Gong et al.
130 2003). These mice carry a bacterial artificial chromosome (BAC) containing an enhanced green
131 fluorescent protein (EGFP) expression cassette which is driven by the *p130Cas* promoter along
132 with its regulatory sequences, thereby causing all cells with *p130Cas* promoter activity to
133 accumulate cytosolic EGFP in a pattern that recapitulates endogenous gene expression (Vahedi-
134 Hunter et al. 2018; Wong et al. 2023).

135 We collected *p130Cas-EGFP-BAC* embryos at E14.5 and E16.5 and neonates at postnatal
136 day 0 (P0) and performed immunohistochemistry for EGFP and Neural Cell Adhesion Molecule
137 L1 (NCAM-L1) (Fischer et al. 1986; Moos et al. 1988; Munakata et al. 2003) to visualize cortical
138 white matter tracts (**Figure 1**). At E14.5, we found *p130Cas*-driven EGFP signal co-expressed
139 with NCAM-L1 in multiple areas: the cortical plate, the lateral cortex, and a group of
140 fasciculating axons forming the presumptive Anterior Commissure (AC) (**Figure 1 A-A''**, white
141 arrowheads denote forming AC). By E16.5, robust *p130Cas*-driven EGFP signal was observed
142 broadly in the cortical plate and the marginal zone (**Figure 1 B-B'**). EGFP signal was also

143 detected in white matter, with clear expression in striatal axons, the External Capsule (EC, **Figure**
144 **1 B**, white asterisk), and the now-midline-crossing AC (**Figure 1 B**, white arrowheads). In
145 neonates (P0), we observed strong *p130Cas*-driven EGFP in all major cortical tracts including the
146 corpus callosum, striatum, EC, and AC (**Figure 1 C-C''**, white asterisk denotes EC and white
147 arrowheads denote AC). Higher-magnification images of *p130Cas-EGFP-BAC* neonates at the
148 pallial-subpallial boundary (PSPB) revealed many diffuse NCAM-L1+ processes innervating the
149 subpallium that were not expressing *p130Cas*-driven EGFP, although many EGFP+ cell bodies
150 occupied this region (**Figure 1 D-D''**, white dotted line indicates boundary). In the cingulate
151 cortex, high-magnification images of P0 *p130Cas*-EGFP-BAC animals showed robust expression
152 of EGFP in the cortical plate and the corpus callosum (**Figure 1 E-E''**).

153 Having confirmed the developmental expression of *Cas* genes during the formation of
154 cortical white matter, we next sought to test the requirement of Cas proteins during cortical
155 tract formation. To this end, we generated *Cas* triple conditional knockouts (*Cas TcKO*)
156 (Riccomagno et al. 2014; Vahedi-Hunter et al. 2018; Wong et al. 2023) to assess the broad
157 requirements for Cas proteins during cortical tract development. In brief, these animals bear
158 homozygous null alleles for the Cas homologues *CasL* (*CasL*$^{-/-}$) and *Sin* (*Sin*$^{-/-}$) while also
159 harboring one floxed allele and one deletion (delta) allele for *p130Cas* (*p130Cas*$^{fl/\Delta}$). Constitutive
160 deletion of *p130Cas* results in early embryonic lethality due to defects in cardiovascular
161 development (Honda et al. 1998). Thus, crossing TcKO animals to cell-specific Cre-driver lines
162 permits Cre-mediated excision of *p130Cas* in neural tissue only, allowing embryos to survive
163 through development.

164 To determine the requirement of *Cas* genes during cortical white matter tract formation,
165 we chose to first induce a broad deletion of *Cas* gene function by crossing *Cas TcKO* animals with
166 *Nestin-Cre* mice. *Nestin-Cre* drives early (E9.5) recombination in neural stem cells and
167 intermediate progenitors (Tronche et al. 1999). As such, *Nestin-Cre* is often employed to
168 produce CNS-wide deletions in both neuronal and glial populations. We generated *Nestin-*
169 *Cre;CasL*$^{-/-}$*;Sin*$^{-/-}$*;p130Cas*$^{fl/\Delta}$ (or more simply *Nes-Cre;TcKO*) mutants and performed
170 immunohistochemistry at P0 for the axon marker NCAM-L1 to examine the organization of
171 major cortical tracts (**Figure 2**). We observed notable disruptions to two major white matter
172 tracts in *Nes-Cre;TcKO* mutants: the Anterior Commissure (AC) and cortical white matter.

173 Axons of the External Capsule (EC) that, upon exit from the pallium, normally turn
174 medially to join the posterior Anterior Commissure (pAC), fail to fasciculate properly in *Nes-*
175 *Cre;TcKO* mutants, and instead project ventrally into the subpallium (**Figure 2 A' and B'**). Tracing
176 experiments using DiA crystals placed into the Somatosensory 2 (S2) region of the cortex
177 (**Supplemental Figure 1 A-B'**) confirmed that these mis-projecting axons originate in the
178 dorsolateral and lateral cortex (**Figure 2 C and D**; n = 6 for *Nes-Cre;TcKO,* n = 7 for controls). We
179 quantified axon pathfinding errors by calculating the average number of stray pAC axon bundles
180 per section per animal in the subpallial area in *Nes-Cre;TcKO* mutants and control mice. The
181 number of stray axon fascicles in the subpallial area in *Nes-Cre;TcKO* animals averaged 4.23 ±
182 1.12, while the average was 0 for control mice (**Figure 2 I**; Unpaired *t*-test, p = 0.0004, n = 7 for
183 *Nes-Cre;TcKO,* n = 10 for controls

184 *Nes-Cre;TcKO* mutants also display severe defects in white matter within the cortical
185 plate, with large bundles of axons mis-projecting towards the pial surface (**Figure 2 A'' and B''**).

186 We hereafter refer to these ectopic projections as Cortical Bundles (CBs). To quantify the CB
187 phenotype, we calculated the average number of CBs present per section per animal in the
188 cortex of both *Nes-Cre;TcKO* mutants and control mice. On average, we observed 7.88 ± 0.72
189 CBs in the cortex of *Nes-Cre;TcKO* and 0 in littermate controls (**Figure 2 J**; Unpaired *t*-test, $p <$
190 0.0001, n = 8 for *Nes-Cre;TcKO,* n = 7 for controls). The cortex receives input from multiple
191 cortical and subcortical areas, including contralateral connections via the corpus callosum and
192 AC (Chédotal and Richards 2010) and thalamic connections from Thalamocortical axon (TCA)
193 projections (López-Bendito and Molnár 2003; Hanashima et al. 2006). We therefore asked if the
194 CB phenotype presented by *Nes-Cre;TcKO* mutants consisted of axons originating from cortical
195 or subcortical areas. Initial tracing experiments using DiA crystals placed into the S2 cortex
196 indicated that mis-projecting axons in CBs are not cortical in origin (**Figure 2 E-F**). We performed
197 additional lipophilic tracing experiments by placing DiI crystals into the laterodorsal nucleus of
198 the thalamus (**Supplemental Figure 1 C-D'**) and found robust labeling of CBs in the ipsilateral
199 hemisphere in *Nes-Cre;TcKO* mutant neonates (**Figure 2 E and F**; n = 6 for *Nes-Cre;TcKO,* n = 5 for
200 controls). This suggests that CBs form primarily from TCA afferents. Taken together, these data
201 point to a strong requirement for *Cas* family genes during cortical white matter tract formation.

202 To examine the developmental progression of *Nes-Cre;TcKO* white matter tract defects,
203 we collected mutant embryos at E14.6, E16.5, and E18.5 and performed immunohistochemistry
204 for NCAM-L1 (**Figure 3**). Interestingly, we observed different developmental trajectories for each
205 mutant phenotype. Initial formation of the EC-AC tract was unperturbed in *Nes-Cre;TcKO*
206 animals with no observable axon defasciculation at E14.5 and E16.5 (**Figure 3 A' and B', C' and**
207 **D'**; E14.5: n = 4 for *Nes-Cre;TcKO,* n = 4 for controls; E16.5: n = 8 for *Nes-Cre;TcKO,* n = 12 for

208 controls). It was not until late embryonic development (E18.5) that we detected aberrant axon
209 defasciculation in the AC (**Figure 3 E' and F'**, white arrowhead), with *Nes-Cre;TcKO* mutants
210 averaging 6.55 ± 1.09 stray axons in the subpallial area, while control animals averaged 0 (**Figure**
211 **3 G**; Unpaired *t*-test, p = 0.0011, n = 5 for *Nes-Cre;TcKO,* n = 4 for controls). In contrast, the CB
212 phenotype is apparent in *Nes-Cre;TcKO* mutants as early as E14.5 (**Figure 3 A'' and B''**, white
213 asterisks), with the phenotype growing in severity as development continued (**Figure 3 C''-F''**,
214 white asterisks denote CBs). The average number of CBs in *Nes-Cre;TcKO* mutant mice increased
215 with age (4.29 ± 0.79 vs 5.06 ± 0.23 vs 9.06 ± 0.76), and at each embryonic time point, the
216 number of CBs observed on average in *Nes-Cre;TcKO* mutants was significantly higher compared
217 to littermate controls (**Figure 3 H**; two-way ANOVA, p < 0.0001; Tukey honestly significant
218 difference (HSD) post hoc test, p < 0.0001 E14.5 *Nes-Cre;TcKO* versus control, E16.5 *Nes-*
219 *Cre;TcKO* versus control, E18.5 *Nes-Cre;TcKO* versus control, E14.5 *Nes-Cre;TcKO* versus E18.5
220 *Nes-Cre;TcKO*, E16.5 *Nes-Cre;TcKO* versus E18.5 *Nes-Cre;TcKO*; ns E14.5 *Nes-Cre;TcKO* vs E16.5
221 *Nes-Cre;TcKO*; E14.5: n = 4 for *Nes-Cre;TcKO,* n = 4 for controls; E16.5: n = 8 for *Nes-Cre;TcKO,* n =
222 12 for controls; E18.5: n = 5 for *Nes-Cre;TcKO,* n = 4 for controls). These results suggest different
223 developmental trajectories for each of the presented white matter tract mutant phenotypes.

224 We next asked if *Cas* family genes are functioning in a cortical-autonomous and
225 neuronal-autonomous manner during establishment of the EC-AC and TCA tracts. With this
226 aim, we generated two new classes of *Cas TcKO* mutants by crossing TcKO animals into *Emx1-Cre*
227 (Gorski et al. 2002) and *Nex-Cre* (Goebbels et al. 2006) driver lines. In contrast to the broad CNS
228 expression of *Nestin-Cre*, *Emx1-Cre* and *Nex-Cre* recombination events are largely restricted to
229 the cortex. *Emx1-Cre* induces recombination in cortical radial glial cells (RGCs), affecting RGCs,

230 cortical excitatory neurons, and macroglial populations, while *Nex-Cre* is active only in early
231 postmitotic excitatory neurons within the cortex. We have previously validated that *Emx1-*
232 *Cre;TcKO* and *Nex-Cre;TcKO* mutant animals do not produce functional *Cas* transcripts in the
233 expected neural populations (Wong et al. 2023).

234 We initially generated *Emx1-Cre;CasL*$^{-/-}$*;Sin*$^{-/-}$ *;p130Cas*$^{fl/\Delta}$ (*Emx1-Cre;TcKO*) mutants and
235 collected neonates (P0) for immunohistochemistry using the axon marker NCAM-L1 (**Figure 4 A-**
236 **B''**). We observed defasciculation of AC axons in *Emx1-Cre;TcKO* animals, which phenocopied
237 the AC defasciculation errors in *Nes-Cre;TcKO* neonates (**Figure 4 A' and B'**). These
238 defasciculating AC axons were labeled by lipophilic tracing from DiA crystals that were placed in
239 the S2 region of the cortex (**Figure 4 C and D**; n = 4 for *Emx1-Cre;TcKO,* n = 5 for controls). In
240 *Emx1-Cre;TcKO* mutants, we observed an average of 7.90 ± 1.43 stray axons in the subpallial
241 area, while in control mice we observed 0 (**Figure 4 M**; Unpaired *t*-test, $p < 0.0001$, n = 8 for
242 *Emx1-Cre;TcKO,* n = 10 for controls). *Emx1-Cre;TcKO* animals also presented the ectopic CB
243 phenotype, with large bundles of axons mis-projecting to the pial surface (**Figure 4 A'' and B''**).
244 On average, we observed 9.15 ± 0.43 CBs in *Emx1-Cre;TcKO* mice and 0 in controls (**Figure 4 N**;
245 Unpaired *t*-test, $p < 0.0001$, n = 8 for *Emx1-Cre;TcKO,* n = 10 for controls). Lastly, we performed
246 axon tracing experiments by placing DiI crystals into the thalamus of *Emx1;TcKO* neonates and
247 confirmed that these CBs are primarily formed by thalamic axons (**Figure 4 E and F**; n = 3 for
248 *Emx1-Cre;TcKO,* n = 3 for controls).

249 Our initial analysis showed that the CBs in *Nes-Cre;TcKO* mutants are primarily TCA
250 afferents originating from the thalamic nuclei (**Figure 2 G and H**). However, *Emx1-Cre* is not
251 expressed in the thalamic territory (Gorski et al. 2002). Thus, the observation of CBs in *Emx1-*

252 *Cre;TcKO* mutants excludes the possibility of a thalamic-autonomous role for *Cas* genes in TCA
253 innervation, thereby demonstrating that the white matter tract phenotypes in *Cas TcKO* animals
254 are cortical-autonomous (i.e. requiring *Cas* gene function in the cortical plate itself).

255 Next, we generated *Nex-Cre;CasL*$^{-/-}$*;Sin*$^{-/-}$*;p130Cas*$^{fl/\Delta}$ (*Nex-Cre;TcKO*) mice and collected
256 neonates (P0) for immunohistochemistry using the axon marker NCAM-L1 (**Figure 4 G-H''**). In
257 contrast to *Emx1-Cre;TcKO* mutants and *Nestin-Cre;TcKO* mutants, *Nex-Cre;TcKO* mutants only
258 presented the AC defasciculation phenotype (**Figure 4 G' and H'**, white arrowheads),
259 demonstrating a neuronal-autonomous role for *Cas* genes during AC fasciculation. These stray
260 AC axons were again confirmed to be dorsolateral and lateral in origin by lipophilic tracing from
261 DiA crystal placement into the S2 cortex (**Figure 4 I and J**, white arrowheads; n = 5 for *Nex-*
262 *Cre;TcKO,* n = 4 for controls) We observed an average of 8.92 ± 1.17 stray axons on the subpallial
263 area of *Nex-Cre;TcKO* mutants and 0 in control mice (Unpaired *t*-test, $p < 0.0001$, n = 7 for *Nex-*
264 *Cre;TcKO,* n = 5 for controls) (**Figure 4 O**). Interestingly, *Nex-Cre;TcKO* mutant neonates do not
265 present the CB phenotype, indicating a non-neuronal autonomous role of *Cas* genes in TCA
266 projections (**Figure 4 G'' and H''**; n = 7 for *Nex-Cre;TcKO,* n = 5 for controls)

267 Analyses of the three classes of *Cas TcKO* mutants thus indicate a complex requirement
268 for *Cas* genes during cortical white matter tract formation. The proper fasciculation of AC axons
269 appears to require *Cas* in a neuronal-autonomous manner, likely reflecting a requirement for
270 *Cas* genes in the projecting axons themselves. In contrast, the proper projection of TCA afferents
271 into the cortex appears to have a non-neuronal-autonomous requirement for *Cas* genes. As
272 such, we infer that *Cas* genes are required by some non-neuronal cortical cell population to

273 properly coordinate TCA guidance, possibly by controlling the positioning of intermediate target
274 populations or the provision of local guidance cues in the cortex.

275 To further assess the cortical- and neuronal-autonomous role of Cas genes during AC
276 fasciculation, we genetically labeled AC axons to confirm their cortical origins. This facilitated a
277 closer examination of their relationship to neighboring tracts. To this end, we made use of the
278 *Ai14/R26*$^{LSL\text{-}tdTomato}$ *Cre* reporter line (or simply *Ai14*) which expresses tdTomato fluorescent
279 protein upon Cre-mediated excision of upstream translational STOP sequences, permitting
280 visualization of cells or tissues that have or previously had Cre recombinase expression
281 (Madisen et al. 2010). We crossed the *Ai14* reporter line into *Emx1-Cre;TcKO* line to generate
282 *Emx1-Cre;Ai14*$^{+/-}$*;TcKO* mutants and collected P0 neonates for immunohistochemistry with the
283 marker NCAM-L1 (**Figure 5 A-D''**). As expected, we found robust labeling of the EC-AC tract in
284 *Emx1-Cre;Ai14*$^{+/-}$ controls (*Emx1-Cre;Ai14*$^{+/-}$*;CasL*$^{+/-}$*;Sin*$^{+/-}$*;p130Cas*$^{+/+}$) and observed tight
285 fasciculation of the AC tract in these animals (**Figure 5 A-B**). Examination of *Emx1-Cre;Ai14*$^{+/-}$
286 *;TcKO* mutants revealed that 100% of the large, defasciculating AC axon bundles were
287 tdTomato+, genetically confirming the cortical origin of these mis-projecting axons (**Figure 5 D-**
288 **D''**, white arrowheads). On average, we observed 9.5 ± 0.29 stray axons in the subpallial area of
289 *Emx1-Cre;Ai14*$^{+/-}$*;TcKO* mice and 0 in *Emx1-Cre;Ai14*$^{+/-}$ controls (**Figure 5 I**; Unpaired *t*-test $p <$
290 0.0001, $n = 3$ for *Emx1-Cre;Ai14*$^{+/-}$*;TcKO*, $n = 3$ for controls) Interestingly, we also observed
291 tdTomato-/NCAM-L1+ processes that diffusely populated the subpallium. The thicker bundles of
292 tdTomato+/NCAM-L1+ processes appeared to interpolate with these tdTomato-/NCAM-L1+
293 processes, (**Figure 5 D**), suggesting that Cas-deficient tdTomato+ axons might be improperly
294 associating with other axonal processes.

295 We next crossed the *Ai14* reporter line into the *Nex-Cre;TcKO* line to generate
296 *NexCre;Ai14*$^{+/-}$*;TcKO* mutants and collected P0 neonates for immunohistochemistry with the
297 marker NCAM-L1 (**Figure 5 E-H''**). As observed with *Emx1-Cre;Ai14*$^{+/-}$ controls, we found robust
298 labeling of the EC-AC tract in *Nex-Cre;Ai14*$^{+/-}$ controls (*Nex-Cre;Ai14*$^{+/-}$*;CasL*$^{+/-}$*;Sin*$^{+/-}$*;p130Cas*$^{+/+}$)
299 (**Figure 5 E-F**). In *Nex-Cre;Ai14*$^{+/-}$*;TcKO* mutants, we observed large, defasciculating AC axon
300 bundles in the subpallial area, 100% of which were tdTomato+ (**Figure 5 H-H''**, white
301 arrowheads). On average, we observed 9.33 ± 2.03 stray axons in the subpallial area in *Nex-*
302 *Cre;Ai14*$^{+/-}$*;TcKO,* while in *Nex-Cre;Ai14*$^{+/-}$ controls we observed 0 (**Figure 5 J**; Unpaired *t*-test p =
303 0.0116, n = 4 for *Nex-Cre;Ai14*$^{+/-}$*;TcKO,* n = 3 for controls). As in *Emx1-Cre;Ai14*$^{+/-}$*;TcKO* mutants,
304 the defasciculating tdTomato+/NCAM-L1+ AC processes in *Nex-Cre;Ai14*$^{+/-}$*;TcKO* mutants
305 appeared to interpolate with the tdTomato-/NCAM-L1+ bundles that also populate the
306 subpallium (**Figure 5 H**). Taken together, these data genetically confirm the cortical origins of
307 defasciculating axons in the AC while also corroborating the neuronal-autonomous role of *Cas*
308 genes for proper AC fasciculation.

309 During canonical adhesion signaling events, Cas proteins are recruited to early Integrin
310 Adhesion Complexes (IACs) via β1-integrin receptor stimulation and subsequent activation of
311 the non-receptor tyrosine kinases Focal Adhesion Kinase (FAK) and Src (Defilippi et al. 2006). In
312 the mammalian brain, β1-integrin, encoded by *Itgb1*, appears to be the most prevalent β
313 subunit involved in mediating adhesion signaling events (Milner and Campbell 2002; Myers et
314 al. 2011; Lilja and Ivaska 2018; Jaudon et al. 2021; Yan and Cui 2023), with established roles in
315 axonal guidance and growth cone dynamics (Bixby and Harris 1991; Renaudin et al. 1999; Myers
316 et al. 2011; Kerstein et al. 2015). To investigate whether β1-integrin could be the adhesion

317 receptor acting upstream of Cas proteins during cortical white matter tract development, we
318 asked if the requirement for *Cas* genes in AC fasciculation and TCA projection was also observed
319 in *Itgb1* mutants.

320 We therefore generated *Emx1-Cre;Itgb1*$^{fl/fl}$ and *Nex-Cre;Itgb1*$^{fl/fl}$ mice and performed
321 immunohistochemistry in neonates (P0) using the axon marker NCAM-L1 (**Figure 6**). We
322 observed bundles of mis-projecting axons in the cortices of *Emx1-Cre;Itgb1*$^{fl/fl}$ mutants, a defect
323 that strongly phenocopied the CB phenotype presented by *Emx1-Cre;Cas TcKO* mutants (**Figure**
324 **6 A'' and B''**, white asterisks). On average, we observed 8.08 ± 0.25 CBs in *Emx1-Cre;Itgb1*$^{fl/fl}$
325 compared to controls which had 0 (**Figure 6 E**; Unpaired *t*-test, $p < 0.0001$, n = 6 for *Emx1-*
326 *Cre;Itgb1*$^{fl/fl}$, n = 5 for controls). *Nex-Cre;Itgb1*$^{fl/fl}$ mutants did not display cortical bundles (**Figure**
327 **6 C'' and D''**; n = 3 for *Nex-Cre;Itgb1*$^{fl/fl}$ mutants, n = 4 for controls). These results suggest a
328 similar non-neuronal-autonomous role for β1-integrin and Cas proteins during TCA projection
329 pathfinding. We also examined the AC commissure tract in *Emx1-Cre;Itgb1*$^{fl/fl}$ and *Nex-*
330 *Cre;Itgb1*$^{fl/fl}$ neonates. Remarkably, we found that neither class of *Itgb1* mutants phenocopied
331 the AC defasciculation defects observed in *Cas TcKO* mutants (**Figure 6 A', B', C' and D'**; n = 6 for
332 *Emx1-Cre;Itgb1*$^{fl/fl}$, n = 5 for controls; n = 3 for *Nex-Cre;Itgb1*$^{fl/fl}$ mutants, n = 4 for controls).
333 These observations demonstrate that the β1-integrin receptor by itself is dispensable for AC
334 fasciculation, suggesting a different receptor may be acting upstream of *Cas* genes during AC
335 formation.

336 Lastly, we sought to identify a developmental mechanism by which TCA afferents mis-
337 project to form CBs in *Cas TcKO* mutants. Previous research from our lab established a role for
338 Cas proteins and β1-integrin during cortical lamination (Wong et al. 2023). We therefore asked if

339 the cortical-autonomous, non-neuronal-autonomous CB phenotype presented by *Emx1-*
340 *Cre;TcKO* and *Emx1-Cre;Igtb1*$^{fl/fl}$ mutants was a secondary phenotype that resulted from the
341 disruption of cortical lamination in these mutants. As previously mentioned, the subplate is a
342 transient structure that acts as an intermediate target for TCAs, coordinating the entry of these
343 thalamic axons into the cortical plate (Ghosh and Shatz 1992; López-Bendito and Molnár 2003).
344 Given the cortical requirement of *Cas* genes for TCA guidance, and the defects in cortical
345 lamination presented by *Cas TcKO* mutants (Wong et al. 2023), we hypothesized that one
346 possible explanation for the CB phenotype presented by our mutants here could be the
347 displacement of subplate and other deep layer neurons in *Emx1-Cre;TcKO* and *Emx1-Cre;Igtb1*$^{fl/fl}$
348 mutants.

349 Thus, we performed immunohistochemistry at E16.5 and P0 in *Emx1-Cre;TcKO* and
350 *Emx1-Cre;Itgb1*$^{fl/fl}$ mutants, using the markers NCAM-L1 and Tbr1 (**Figure 7 and Figure 8**,
351 respectively). Tbr1 is a transcription factor known to regulate the specification of the subplate
352 and layer VI cortical layers (Hevner et al. 2001). Indeed, we found, at E16.5 and P0, both *Emx1-*
353 *Cre;TcKO* and *Emx1- Cre;Itgb1*$^{fl/fl}$ mutants displayed cortical dysplasia, as previously described
354 (Wong et al. 2023): lamination of deep-layer Tbr1+ cells is highly disrupted, with columns of
355 Tbr1+ cells reaching the marginal zone (**Figure 7 B and D, F and H**; **Figure 8 B and D, F and H**).
356 Interestingly, in both *Emx1-Cre;TcKO* and *Emx1-Cre;Itgb1*$^{fl/fl}$ mutants, 100% of the NCAM-L1+
357 CBs associated with these displaced Tbr1+ cells, at times with clear "tunnels" of Tbr1+ cells
358 containing CBs mis-projecting to the marginal zone (**Figure 7 D-D'', H-H''**, white asterisks; **Figure**
359 **8 D-D'', H-H''**, white asterisks). These results demonstrate that the disorganization of the

360 subplate and deep cortical layers observed in both pan-cortical *Cas TcKO* and *Itgb1* mutant mice
361 strongly correlates with the ectopic CB phenotype in these animals.

362

363 **Discussion**

364 In this study, we used conditional mouse genetics to assess the cortical-autonomous and
365 neuronal-autonomous roles of *Cas* genes during forebrain white matter tract formation. Using a
366 *Cas* triple conditional knockout (*Cas TcKO*) model, we provide strong genetic evidence that Cas
367 proteins are required in two manners: 1) cortical- and neuronal-autonomously for proper
368 fasciculation of the posterior branch of the Anterior Commissure (pAC) (**Figure 2 B' and D**), and
369 2) cortical- and non-neuronal autonomously for thalamocortical axon (TCA) guidance (**Figure 2**
370 **B'' and H**).

371 The AC is a highly evolutionarily conserved forebrain tract that, in mice, makes reciprocal
372 connections between the Anterior Olfactory Nuclei of each olfactory bulb (via the anterior AC
373 tract, aAC) and mediates reciprocal connections between the piriform and entorhinal cortices of
374 the two hemispheres (via the posterior AC tract, pAC) (Fenlon et al. 2021). Recent
375 developmental studies have identified a small group of pioneering axons with unusual
376 elongation kinetics that advance towards the embryonic midline at E13, preceding the majority
377 of pAC axons that arrived later at E15 (Martin-Lopez et al. 2018). These later arriving processes
378 join the stalled pioneers to form a primary fascicle that crosses the embryonic midline in unison
379 at E16, then innervates contralaterally and achieves specific target selection at E17 and E18,
380 respectively (Martin-Lopez et al. 2018). In our study, we find that *Cas TcKO* mutants display

381 defasciculation and ventral targeting of axons of the pAC tract (**Figure 2 B' and D**). However,
382 these defects are only observable at later embryonic (E18.5) and postnatal (P0) stages (**Figure 3**
383 **F** and **Figure 2 B**). Considering the timeline of pAC formation, this suggests that the axons that
384 fail to fasciculate properly are a population of late "follower" axons arriving at the AC later in
385 development.

386 Interestingly, we find that the defasciculating AC processes originate from the
387 dorsolateral cortex, as they are labeled by lipophilic tracing from the somatosensory S2 cortex in
388 all three classes of *Cas TcKO* mutants analyzed (**Figure 2 D**; **Figure 4 D and J**). These results are
389 somewhat unexpected: the pAC has been primarily described as carrying axons from
390 ventrolateral cortical areas in mice (Fenlon et al. 2021). The observation of DiI-labeled AC axons
391 in both control and mutant animals after placement of dye crystals in S2 might suggest that a
392 population of cortical axons projecting along the EC contributes to the formation of the AC.
393 However, we cannot exclude the possibility that DiI cross-labeled other AC-projecting cortical
394 axons ventral to S2. We genetically confirmed the cortical origin of the defasciculating AC axons
395 using the *Ai14 Cre*-dependent reporter in both the *Emx1-Cre* and *Nex-Cre* lines (**Figure 5**).
396 Additionally, we observed interpolation of defasciculating tdTomato+ AC processes with other
397 tdTomato-/NCAM-L1+ processes in the subpallium. This may suggest that these defasciculating
398 axons may be failing to properly regulate homotypic versus heterotypic associations (Spead and
399 Poulain 2020). Taken together, these data support a neuronal cell-autonomous requirement of
400 *Cas* genes for the guidance of a subset of cortical axons, that in the absence of these genes, mis-
401 project into the ventral subpallium.

402 During canonical adhesion signaling, Cas proteins are recruited to IACs following integrin
403 receptor activation (Vuori et al. 1996; Defilippi et al. 2006; Donato et al. 2010). The integrins are
404 a large family of transmembrane receptors that include 18 alpha (α) and 8 beta (β) subunits and
405 are known to form 24 combinations of αβ heterodimers (Schwartz 2001; Takada et al. 2007).
406 The β1-integrin subunit has been particularly well studied and is found in 12 of the known
407 heterodimer combinations, mediating many intracellular signaling functions during CNS
408 development (Hynes 1992; Milner and Campbell 2002; Schmid and Anton 2003; Takada et al.
409 2007; Myers et al. 2011; Riccomagno et al. 2014; Lilja and Ivaska 2018; Jaudon et al. 2021). We
410 therefore analyzed the structure of the AC in *Igtb1* mutant neonates which are deficient for the
411 β1-integirn subunit. Surprisingly, conditional deletion of *Igtb1* using *Emx1-Cre* or *Nex-Cre* failed
412 to phenocopy the AC defasciculation defects observed in *Cas TcKO* mutants (**Figure 6**),
413 suggesting that β1-integrin is dispensable for proper fasciculation of this tract. This raises two
414 intriguing possibilities: 1) there is compensation by another β subunit in *Igtb1* deficient mice, or
415 2) Cas proteins are signaling downstream of a different type of receptor.

416 In support of the first possibility, β5-integrin, β6-integrin, and β8-integrin are expressed
417 in the embryonic cortex (Schmid and Anton 2003). Thus, they might be acting as part of the
418 adhesion receptors driving the fasciculation of the AC axons, or might compensate for the loss
419 of *Igtb1* in mutant mice via the formation of heterodimers with α-integrins. For example,
420 heterodimer formation between αV-integrin and β1-, β5-, β6-, and β8-integrin has been
421 previously documented (Takada et al. 2007). Of all α-subunits, αV-integrin appears as a prime
422 candidate to modulate this process: in addition to being able to form heterodimers with
423 multiple β-integrins, αV-integrin is known to have a critical role in neurodevelopment and is

424 expressed in axons of white matter tracts in the cerebral cortex (McCarty et al. 2005; Denda and
425 Reichardt 2007). Moreover, αV-integrin containing dimers bind to the ECM molecules laminin,
426 fibronectin, vitronectin, tenascin, and collagen (Schmid and Anton 2003; Lilja and Ivaska 2018).
427 Importantly, laminin, fibronectin, and tenascin are expressed by a population of midline glial
428 cells that help coordinate the development of the pAC (Pires-Neto et al. 1998). One possible
429 scenario then is that β5-integrin, β6-integrin, or β8-integrin are acting as functional partners
430 with αV-integrin during AC fasciculation, or can at least compensate for the loss of *Igtb1.*

431 The second possible explanation for the failure of *Igtb1* mutants to phenocopy the AC
432 defasciculation defects presented by *Cas TcKO* animals is that Cas proteins are signaling
433 downstream of an entirely different receptor system. It has previously been shown that
434 phospho-activation of Cas can be modulated by CXCL12/CXCR4 (Wang et al. 2000), Neuropilin
435 (Evans et al. 2011), Netrin (Liu et al. 2007), and Eph/Ephrin (Bourgin et al. 2007) signaling.
436 Moreover, mutations in several genes that participate in these signaling pathways or have
437 known roles in adhesion have been shown to affect the development of the AC. aAC
438 development is abnormal in *DCC* mutant animals (Fazeli et al. 1997); formation of the pAC is
439 affected in *Ephb2/Nuk* (Henkemeyer et al. 1996), *Ephb1/Ephb2* (Robichaux et al. 2016), and
440 *p35/Cdk5r1* (Kwon et al. 1999) null mice; and the entire AC tract is disrupted in mice carrying
441 loss-of-function mutations for *Draxin* (Islam et al. 2009), *Tsku* (Ito et al. 2010), *Schip1* (Klingler et
442 al. 2015), *Ntn1* (Netrin-1) (Serafini et al. 1996), *Sema3b* (Falk et al. 2005), *Sema3f* (Sahay et al.
443 2003), *Epha4/Sek* (Dottori et al. 1998), *Plxna4* (Suto et al. 2005), *Nrp2* (Neuropilin 2) (Chen et al.
444 2000; Giger et al. 2000), *Islr2/Linx* (Abudureyimu et al. 2018), *Dcx/Dclk1* (Deuel et al. 2006),
445 *Fgfr1* (Tole et al. 2006), *Celsr2* (Qu et al. 2014), *Celsr3* (Tissir et al. 2005), *Robo1/Robo2* (López-

446 Bendito et al. 2007), *Fzd3* (Hua et al. 2014), *Gap43* (Shen et al. 2002), and *Rac1* (Chen et al.
447 2007). However, most of these mutations result in thinning or absence of the AC tracts, not
448 defasciculation of AC axons.

449 Notably, *Ephb2/Nuk* mutants (Henkemeyer et al. 1996) and *Ephb1/Ephb2* double-
450 mutants (Robichaux et al. 2016) display defasciculation and ventral targeting of pAC axons, that
451 partially phenocopy *Cas TcKO* mutants. Moreover, biochemical studies have implicated cross-
452 talk between β1-integrin and EphB/EphrinB receptor pathways in various cell types (Stein et al.
453 1998a, b; Huynh-Do et al. 1999; Becker et al. 2000), including retinal ganglion cells (Suh et al.
454 2004) and mossy fiber axons (Xu and Henkemeyer 2009). It is possible that these signaling
455 cascades may be coordinating phosphorylation of Cas proteins in cortical neuron axons as well.
456 Determining whether Cas proteins are working downstream of Eph/Ephrin receptor systems
457 during AC projection and fasciculation will be an interesting goal for future studies.

458 The second white matter tract phenotype presented by *Cas TcKO* mutants is the
459 appearance of large ectopic bundles of axons mis-projecting towards the pial surface of the
460 cortex (**Figure 2 A'' and B''**), which we termed Cortical Bundles (CBs). Lipophilic tracing
461 experiments revealed the origin of these mis-projections to be thalamic (**Figure 2 F and H**).
462 Genetic experiments demonstrated that this phenotype is cortical-autonomous, but non-
463 neuronal-autonomous: conditional deletion of *Cas* genes using *Nex-Cre* fails to recapitulate the
464 CB phenotype (**Figure 4 H'' and L**). From this, we inferred that *Cas* gene function is not required
465 in TCA projections themselves, but rather some cortical-resident population that is responsible
466 for coordinating TCA entry. Additionally, analysis of *Igtb1* mutants also revealed a cortical-

467 autonomous, non-neuronal-autonomous role for β1-integrin. Conditional deletion of *Igtb1*
468 using *Nex-Cre* did not result in the formation of CBs (**Figure 6 D''**).

469 During normal development, TCA innervation of the cortex is regulated by a transient
470 structure known as the subplate which acts as an intermediate target for TCAs until their target
471 layer (layer IV) is fully formed (Molnár et al. 2012). Arriving TCA projections stall in the subplate
472 for several days and grow extensive side processes within the subplate during this waiting
473 period (Ghosh et al. 1990; Allendoerfer and Shatz 1994; Ayoub and Kostovic 2009). Upon
474 entering the cortical plate, TCAs form transient microcircuits with subplate neurons and
475 maturing cortical layer IV neurons, a process which appears to facilitate the proper targeting of
476 layer IV and thus the organization of mature circuits (Kanold and Luhmann 2010; Tolner et al.
477 2012; Viswanathan et al. 2012). Mutations that disrupt the laminar organization of the subplate,
478 such as *reeler* mutants (Molnár et al. 1998b) and *Cdk5* mutants (Gilmore et al. 1998), result in
479 aberrant TCA projection patterns within the cortical plate, speaking to the developmental
480 importance of the subplate in TCA guidance. Previous work from our lab and other labs has
481 demonstrated that *Cas TcKO* and *Igtb1* mutants have severely disrupted laminar organization of
482 the cortex caused by breakages in the basal lamina that destabilize radial glial endfeet
483 attachment, thus resulting in improper migration of cortical neurons and severe cortical
484 dysplasia (Graus-Porta et al. 2001; Belvindrah et al. 2007; Wong et al. 2023).

485 Taking all of this into consideration, in this study, we asked if the disruption of subplate
486 and layer VI organization observed in *Cas TcKO* and *Igtb1* mutants could be a contributing
487 developmental factor to the cortical-autonomous defects we observed in TCA guidance. Indeed,
488 using the subplate/Layer VI marker Tbr1, we observed severe displacement of the deep cortical

489 layers at E16.5 and P0 in both *Cas TcKO* and *Igtb1* mutants (**Figure 7 and Figure 8**). Co-labeling
490 with NCAM-L1 revealed that 100% of ectopic CB projections correlate with sites of displaced
491 Tbr1+ cells (**Figure 7 D and H**, **Figure 8 D and H**). Within the context of our previous work (Wong
492 et al. 2023), these results suggest a model whereby *Cas* genes are required in cortical radial glial
493 cells to regulate endfeet attachment, stabilization of the basement membrane, and glial process
494 organization, which subsequently aid in neuronal migration and formation of the cortical layers,
495 including the subplate. In the absence of *Cas* or *Igtb1* genes, these radial glial tracks are
496 disrupted, resulting in mispositioned subplate neurons (**Figure 7 D and H**, **Figure 8 D and H**;
497 (Wong et al. 2023)). These mispositioned subplate neurons could potentially recruit TCAs for
498 innervation, causing ectopic cortical bundles to innervate the proper intermediate target that is
499 positioned in the wrong location. These results, however indirect, also add to an extensive body
500 of literature suggesting that proper lamination and formation of the subplate is required for
501 appropriate TCA afferent projection (McConnell et al. 1989; Ghosh et al. 1990; Ghosh and Shatz
502 1992; Allendoerfer and Shatz 1994; O'Leary et al. 1994; Molnár et al. 1998a, 2012; López-
503 Bendito and Molnár 2003; Kanold et al. 2003; Kanold 2009; Kanold and Luhmann 2010;
504 Hoerder-Suabedissen and Molnár 2012; López-Bendito 2018; Ohtaka-Maruyama 2020; Molnár
505 and Kwan 2024).

506 Collectively, these studies demonstrate dual roles for the Cas family of signal adaptor
507 proteins functioning neuronal- and non-neuronal-autonomously during axonal guidance and
508 fasciculation of cortical white matter tracts. We build on previous genetic evidence that *Cas*
509 genes function radial glial-autonomously downstream of the β1-integrin receptor to ensure
510 proper lamination of the cortex (Wong et al. 2023), demonstrating that errors in lamination

511 result in disruptions to the subplate. Based on our data, we propose that this misplacement of
512 the subplate might cause aberrant thalamocortical axon guidance and the formation of ectopic
513 bundles that mis-project towards the pial surface. Further, we provide genetic evidence that *Cas*
514 genes function independently of the β1-integrin receptor in a neuronal-autonomous manner
515 during fasciculation and guidance of the Anterior Commissure, demonstrating that a subset of
516 late-arriving axons fail to properly fasciculate with the posterior branch of the Anterior
517 Commissure. These defasciculating axons display improper ventral targeting upon crossing the
518 pallial-subpallial boundary. This study implicates Cas proteins as key mediators of axon
519 fasciculation and pathfinding for cortical white matter tracts, and adds to a growing body of
520 work suggesting essential roles for Cas proteins in adhesion signaling during guidance and
521 migration (Defilippi et al. 2006; Liu et al. 2007; Huang et al. 2007; Cabodi et al. 2010;
522 Riccomagno et al. 2014; Machiyama et al. 2014; Vahedi-Hunter et al. 2018; Wong et al. 2023).

523

524 **Materials & Methods**

525 **Animals and Genotyping:** For embryonic collections, the morning of vaginal plug observation
526 was designated as embryonic day 0.5 (E0.5) and the day of birth was postnatal day 0 (P0). The
527 generation of the *Cas TcKO* model has been previously described (Seo et al. 2005; Donlin et al.
528 2005; Riccomagno et al. 2014). The following lines were purchased from The Jackson
529 Laboratory: *Nestin-Cre* (Stock: 003771), *Emx1-Cre* (Stock: 005628), *Ai14/R26*$^{LSL\text{-}tdTomato}$ (Stock:
530 007914), and *Itgb1*$^{fl/fl}$ (Stock: 004605). Genotyping for *Nestin-Cre* was carried out using the
531 following primers: F: CCT TCC TGA AGC AGT AGA GCA R: GCC TTA TTG TGG AAG GAC TG.

532 Genotyping for *Emx1-Cre* was carried out using the following primers: F: CCA TAT CAA CCG GTG
533 GCG CAT C and R: TCG ATA AGC TTG GAT CCG GAG AG. Genotyping for *Ai14/R26*$^{LSL\text{-}tdTomato}$ was
534 carried out using the following primers: WTF: AAG GGA GCT GCA GTG GAG TA, WTR: CCG AAA
535 ATC TGT GGG AAG TC, MutF: CTG TTC CTG TAC GGC ATG G, and MutR: GGC ATT AAA GCA GCG
536 TAT CC. Genotyping for *Itgb1*$^{fl/fl}$ mice was carried out using the primers: F: CGG CTC AAA GCA
537 GAG TGT CAG TC and R: CCA CAA CTT TCC CAG TTA GCT CTC. *Nex-Cre* mice were kindly provided
538 by Drs. Nave and Goebbels (Wu et al. 2005; Goebbels et al. 2006). Genotyping for *Nex-Cre* was
539 carried out using the following primers: Primer 4: GAG TCC TGG AAT CAG TCT TTT TC, Primer 5:
540 AGA ATG TGG AGT AGG GTG AC, and Primer 6: CCG CAT AAC CAG TGA AAC AG. Tail biopsies
541 were digested with Quanta tail extraction reagent kit (cat: 95091-025) and PCR reactions were
542 prepared using GoTaq Master Mix (Promega cat: PRM7123). All animal procedures were
543 performed according to the University of California, Riverside's Institutional Animal Care and
544 Use Committee (IACUC) guidelines. All procedures were approved by UC Riverside IACUC.

545 **Immunohistochemistry:** Embryos, neonates, and adult mice were transcardially perfused with
546 ice-cold 1xPBS and subsequently dissected in cold 1xPBS. Brain tissue was post-fixed in 4% PFA
547 (diluted in 1xPBS) for 2hrs – overnight at 4°C. Tissue samples were processed immediately as
548 floating sections or cryopreserved in a solution of 30% sucrose in 1xPBS before embedding in
549 Tissue Plus O.C.T. Compound (Fisher HealthCare, cat:4585) for long-term storage. Tissue
550 processed as floating sections was embedded in 3% agarose and sectioned coronally as 100-
551 150µm sections on a vibratome (Lecia, cat: VT1000S). Floating sections were incubated with a
552 permeabilization solution containing 3% bovine serum albumin (BSA) and 0.3% TritonX-100 in
553 1xPBS for 4hrs – overnight at 4°C. Primary and secondary antibody mixes were diluted in a

554 solution of 5% goat serum made with permeabilization solution. All antibody incubations were
555 overnight at 4°C with gentle agitation. Cryoprotected samples were sectioned coronally at 25-
556 50µm on a cryostat (Leica cat: CM3050). Cryosections were dried for 20 minutes at room
557 temperature before blocking in freshly prepared blocking buffer (10% goat serum and 0.1%
558 TritonX-100 in 1xPBS) for 1hr before primary antibody addition. Antibodies were then prepared
559 in blocking buffer with reduced goat serum (5%) and incubated in a humidified chamber
560 overnight at 4°C. The antibodies and concentrations used in this study: chicken anti-GFP (1:500,
561 Aves cat: GFP-1020), rat anti-NCAM-L1 (1:500, Millipore cat: MAB5272), rabbit anti-dsRed
562 (1:500, Takara Bioscience cat: 632496), rabbit anti-Tbr1 (1:500, Abcam cat: ab31940
563 [polyclonal]), and rabbit anti-Tbr1 (1:500, Abcam cat: ab183032 [monoclonal]). Secondary
564 antibodies were purchased from ThermoFisher and diluted to 1:1000 from the stock
565 concentration: goat anti-chicken 488 (cat: A-11039), goat anti-rabbit 546 (cat: A-11035), goat
566 anti-rat 488 (cat: A-21208), goat anti-rat 546 (cat: A-11081). Nuclear counterstain was achieved
567 by co-incubation with 1ug/ml DAPI (ThermoFisher cat: 50850585) in all secondary antibody
568 incubations. Tissue was mounted using Fluorogel with DABCO (Electron Microscopy Sciences,
569 cat:17985-02). Confocal scanning images were acquired on a Leica DMi8 using a 10x objective
570 (NA=0.40) or 20x objective (NA=0.75) and z-stacks were acquired with 20-40 steps of sizes of 2-
571 4µm.

572 **Axonal Tracing:** Lipophilic tracing of white matter tracts was performed by manually placing
573 small crystals of either DiA (Invitrogen cat: D3883) or DiI (Invitrogen cat: D282) into neonate
574 tissue dissected as described above for immunohistochemistry and postfixed in 4% PFA in 1xPBS
575 overnight. Lipophilic crystals were allowed to diffuse for 8 weeks at 37°C in a solution of 4% PFA

576 in 1xPBS, with the solution changed daily for the first 4 days and weekly thereafter. Tissue was
577 embedded in 3% agarose in 1xPBS and sectioned as 150µm sections on a vibratome (Lecia, cat:
578 VT1000S). Sections were imaged freshly sliced on a Zeiss Axio Imager 2 microscope.

579 **Quantification of Stray Axons and Cortical Bundles:** Quantification of stray axons
580 defasciculating from the EC-AC tract and mis-projecting Cortical Bundles (CBs) was done using
581 ImageJ. The number of stray axons in the subpallial area and the number of CBs in the cortex
582 were counted manually for each section per animal using the ImageJ multipoint tool. Graph
583 values are represented as mean ± standard error of mean, with n = 3 to 12 independent animals
584 per group depending on the experiment, and 2 to 12 sections analyzed per animal. The datasets
585 were then tested for normality using the Shapiro–Wilk test and QQ plot. For normally
586 distributed datasets, Unpaired *t*-test was performed for comparing two independent samples,
587 and two-way ANOVA followed by Tukey honestly significant difference (HSD) post hoc test was
588 used for multiple comparisons.

589 **Ethics approval:** All animal procedures presented here were performed according to the
590 University of California, Riverside's Institutional Animal Care and Use Committee (IACUC)-
591 approved guidelines, under protocol A-8.

592 **Acknowledgements**

593 We would like to thank Dr. Teresa Ubina for critically reading the manuscript and providing
594 helpful comments. We would like to thank Drs. Nave and Goebbels for the *Nex-Cre* mice. We
595 would also like to thank Drs. Sachiko Seo and Mineo Kurokawa, and Dr. Konstantina
596 Alexandropoulos for sharing the *CasL*$^{-/-}$ and *Sin*$^{-/-}$ mouse lines, respectively.

Competing interests

The authors declare no competing financial interests.

Availability of data and materials

All data analyzed during this study are included in this article.

Authors Contributions

JAE and AMT designed and performed experiments and wrote the manuscript. PD, PW, and WW designed and performed experiments. MMR conceived the project, designed experiments, and wrote the manuscript.

606 **References**

607 Abudureyimu S, Asai N, Enomoto A, et al (2018) Essential Role of Linx/Islr2 in the Development
608 of the Forebrain Anterior Commissure. Sci Rep 8:7292. https://doi.org/10.1038/s41598-
609 018-24064-0

610 Allendoerfer KL, Shatz CJ (1994) The subplate, a transient neocortical structure: its role in the
611 development of connections between thalamus and cortex. Annu Rev Neurosci 17:185–
612 218. https://doi.org/10.1146/annurev.ne.17.030194.001153

613 Ayoub AE, Kostovic I (2009) New horizons for the subplate zone and its pioneering neurons.
614 Cereb Cortex 19:1705–1707. https://doi.org/10.1093/cercor/bhp025

615 Bargon SD, Gunning PW, O'Neill GM (2005) The Cas family docking protein, HEF1, promotes the
616 formation of neurite-like membrane extensions. Biochim Biophys Acta 1746:143–154.
617 https://doi.org/10.1016/j.bbamcr.2005.10.008

618 Becker E, Huynh-Do U, Holland S, et al (2000) Nck-interacting Ste20 kinase couples Eph
619 receptors to c-Jun N-terminal kinase and integrin activation. Mol Cell Biol 20:1537–1545.
620 https://doi.org/10.1128/MCB.20.5.1537-1545.2000

621 Belvindrah R, Graus-Porta D, Goebbels S, et al (2007) Beta1 integrins in radial glia but not in
622 migrating neurons are essential for the formation of cell layers in the cerebral cortex. J
623 Neurosci 27:13854–13865. https://doi.org/10.1523/JNEUROSCI.4494-07.2007

624 Bixby JL, Harris WA (1991) Molecular mechanisms of axon growth and guidance. Annu Rev Cell
625 Biol 7:117–159. https://doi.org/10.1146/annurev.cb.07.110191.001001

626 Bourgin C, Murai KK, Richter M, Pasquale EB (2007) The EphA4 receptor regulates dendritic
627 spine remodeling by affecting beta1-integrin signaling pathways. J Cell Biol 178:1295–
628 1307. https://doi.org/10.1083/jcb.200610139

629 Bouton AH, Riggins RB, Bruce-Staskal PJ (2001) Functions of the adapter protein Cas: signal
630 convergence and the determination of cellular responses. Oncogene 20:6448–6458.
631 https://doi.org/10.1038/sj.onc.1204785

632 Breau MA, Trembleau A (2023) Chemical and mechanical control of axon fasciculation and
633 defasciculation. Semin Cell Dev Biol 140:72–81.
634 https://doi.org/10.1016/j.semcdb.2022.06.014

635 Cabodi S, del Pilar Camacho-Leal M, Di Stefano P, Defilippi P (2010) Integrin signalling adaptors:
636 not only figurants in the cancer story. Nat Rev Cancer 10:858–870.
637 https://doi.org/10.1038/nrc2967

638 Caudy M, Bentley D (1986) Pioneer growth cone steering along a series of neuronal and non-
639 neuronal cues of different affinities. J Neurosci 6:1781–1795.
640 https://doi.org/10.1523/JNEUROSCI.06-06-01781.1986

641 Chédotal A, Richards LJ (2010) Wiring the brain: the biology of neuronal guidance. Cold Spring
642 Harb Perspect Biol 2:a001917. https://doi.org/10.1101/cshperspect.a001917

643 Chen H, Bagri A, Zupicich JA, et al (2000) Neuropilin-2 regulates the development of selective
644 cranial and sensory nerves and hippocampal mossy fiber projections. Neuron 25:43–56.
645 https://doi.org/10.1016/s0896-6273(00)80870-3

646 Chen L, Liao G, Waclaw RR, et al (2007) Rac1 controls the formation of midline commissures and
647 the competency of tangential migration in ventral telencephalic neurons. J Neurosci
648 27:3884–3893. https://doi.org/10.1523/JNEUROSCI.3509-06.2007

649 Defilippi P, Di Stefano P, Cabodi S (2006) p130Cas: a versatile scaffold in signaling networks.
650 Trends Cell Biol 16:257–263. https://doi.org/10.1016/j.tcb.2006.03.003

651 Denda S, Reichardt LF (2007) Studies on integrins in the nervous system. Methods Enzymol
652 426:203–221. https://doi.org/10.1016/S0076-6879(07)26010-0

653 Deneka A, Korobeynikov V, Golemis EA (2015) Embryonal Fyn-associated substrate (EFS) and
654 CASS4: The lesser-known CAS protein family members. Gene 570:25–35.
655 https://doi.org/10.1016/j.gene.2015.06.062

656 Deuel TAS, Liu JS, Corbo JC, et al (2006) Genetic interactions between doublecortin and
657 doublecortin-like kinase in neuronal migration and axon outgrowth. Neuron 49:41–53.
658 https://doi.org/10.1016/j.neuron.2005.10.038

659 Donato DM, Ryzhova LM, Meenderink LM, et al (2010) Dynamics and mechanism of p130Cas
660 localization to focal adhesions. J Biol Chem 285:20769–20779.
661 https://doi.org/10.1074/jbc.M109.091207

662 Donlin LT, Danzl NM, Wanjalla C, Alexandropoulos K (2005) Deficiency in expression of the
663 signaling protein Sin/Efs leads to T-lymphocyte activation and mucosal inflammation.
664 Mol Cell Biol 25:11035–11046. https://doi.org/10.1128/MCB.25.24.11035-11046.2005

665 Dottori M, Hartley L, Galea M, et al (1998) EphA4 (Sek1) receptor tyrosine kinase is required for
666 the development of the corticospinal tract. Proc Natl Acad Sci U S A 95:13248–13253.
667 https://doi.org/10.1073/pnas.95.22.13248

668 Easter SS, Burrill J, Marcus RC, et al (1994) Initial tract formation in the vertebrate brain. Prog
669 Brain Res 102:79–93. https://doi.org/10.1016/S0079-6123(08)60533-6

670 Easter SS, Ross LS, Frankfurter A (1993) Initial tract formation in the mouse brain. J Neurosci
671 13:285–299. https://doi.org/10.1523/JNEUROSCI.13-01-00285.1993

672 Evans IM, Yamaji M, Britton G, et al (2011) Neuropilin-1 signaling through p130Cas tyrosine
673 phosphorylation is essential for growth factor-dependent migration of glioma and
674 endothelial cells. Mol Cell Biol 31:1174–1185. https://doi.org/10.1128/MCB.00903-10

675 Falk J, Bechara A, Fiore R, et al (2005) Dual functional activity of semaphorin 3B is required for
676 positioning the anterior commissure. Neuron 48:63–75.
677 https://doi.org/10.1016/j.neuron.2005.08.033

678 Fazeli A, Dickinson SL, Hermiston ML, et al (1997) Phenotype of mice lacking functional Deleted
679 in colorectal cancer (Dcc) gene. Nature 386:796–804. https://doi.org/10.1038/386796a0

680 Fenlon LR, Suarez R, Lynton Z, Richards LJ (2021) The evolution, formation and connectivity of
681 the anterior commissure. Semin Cell Dev Biol 118:50–59.
682 https://doi.org/10.1016/j.semcdb.2021.04.009

683 Fischer G, Künemund V, Schachner M (1986) Neurite outgrowth patterns in cerebellar
684 microexplant cultures are affected by antibodies to the cell surface glycoprotein L1. J
685 Neurosci 6:605–612. https://doi.org/10.1523/JNEUROSCI.06-02-00605.1986

686 Fonseca PM, Shin N-Y, Brábek J, et al (2004) Regulation and localization of CAS substrate domain
687 tyrosine phosphorylation. Cell Signal 16:621–629.
688 https://doi.org/10.1016/j.cellsig.2003.10.004

689 Garel S, López-Bendito G (2014) Inputs from the thalamocortical system on axon pathfinding
690 mechanisms. Curr Opin Neurobiol 27:143–150.
691 https://doi.org/10.1016/j.conb.2014.03.013

692 Ghosh A, Antonini A, McConnell SK, Shatz CJ (1990) Requirement for subplate neurons in the
693 formation of thalamocortical connections. Nature 347:179–181.
694 https://doi.org/10.1038/347179a0

695 Ghosh A, Shatz CJ (1992) Involvement of subplate neurons in the formation of ocular
696 dominance columns. Science 255:1441–1443. https://doi.org/10.1126/science.1542795

697 Giger RJ, Cloutier JF, Sahay A, et al (2000) Neuropilin-2 is required in vivo for selective axon
698 guidance responses to secreted semaphorins. Neuron 25:29–41.
699 https://doi.org/10.1016/s0896-6273(00)80869-7

700 Gilmore EC, Ohshima T, Goffinet AM, et al (1998) Cyclin-dependent kinase 5-deficient mice
701 demonstrate novel developmental arrest in cerebral cortex. J Neurosci 18:6370–6377.
702 https://doi.org/10.1523/JNEUROSCI.18-16-06370.1998

703 Goebbels S, Bormuth I, Bode U, et al (2006) Genetic targeting of principal neurons in neocortex
704 and hippocampus of NEX-Cre mice. Genesis 44:611–621.
705 https://doi.org/10.1002/dvg.20256

706 Gong S, Zheng C, Doughty ML, et al (2003) A gene expression atlas of the central nervous
707 system based on bacterial artificial chromosomes. Nature 425:917–925.
708 https://doi.org/10.1038/nature02033

709 Gorski JA, Talley T, Qiu M, et al (2002) Cortical excitatory neurons and glia, but not GABAergic
710 neurons, are produced in the Emx1-expressing lineage. J Neurosci 22:6309–6314.
711 https://doi.org/10.1523/JNEUROSCI.22-15-06309.2002

712 Graus-Porta D, Blaess S, Senften M, et al (2001) Beta1-class integrins regulate the development
713 of laminae and folia in the cerebral and cerebellar cortex. Neuron 31:367–379.
714 https://doi.org/10.1016/s0896-6273(01)00374-9

715 Gustavsson A, Yuan M, Fällman M (2004) Temporal dissection of beta1-integrin signaling
716 indicates a role for p130Cas-Crk in filopodia formation. J Biol Chem 279:22893–22901.
717 https://doi.org/10.1074/jbc.M309693200

718 Hanashima C, Molnár Z, Fishell G (2006) Building bridges to the cortex. Cell 125:24–27.
719 https://doi.org/10.1016/j.cell.2006.03.021

720 Henkemeyer M, Orioli D, Henderson JT, et al (1996) Nuk controls pathfinding of commissural
721 axons in the mammalian central nervous system. Cell 86:35–46.
722 https://doi.org/10.1016/s0092-8674(00)80075-6

723 Hevner RF, Shi L, Justice N, et al (2001) Tbr1 regulates differentiation of the preplate and layer 6.
724 Neuron 29:353–366. https://doi.org/10.1016/s0896-6273(01)00211-2

725 Hoerder-Suabedissen A, Molnár Z (2012) Morphology of mouse subplate cells with identified
726 projection targets changes with age. J Comp Neurol 520:174–185.
727 https://doi.org/10.1002/cne.22725

728 Honda H, Nakamoto T, Sakai R, Hirai H (1999) p130(Cas), an assembling molecule of actin
729 filaments, promotes cell movement, cell migration, and cell spreading in fibroblasts.
730 Biochem Biophys Res Commun 262:25–30. https://doi.org/10.1006/bbrc.1999.1162

731 Honda H, Oda H, Nakamoto T, et al (1998) Cardiovascular anomaly, impaired actin bundling and
732 resistance to Src-induced transformation in mice lacking p130Cas. Nat Genet 19:361–
733 365. https://doi.org/10.1038/1246

734 Hua ZL, Jeon S, Caterina MJ, Nathans J (2014) Frizzled3 is required for the development of
735 multiple axon tracts in the mouse central nervous system. Proc Natl Acad Sci U S A
736 111:E3005-3014. https://doi.org/10.1073/pnas.1406399111

737 Huang Z, Yazdani U, Thompson-Peer KL, et al (2007) Crk-associated substrate (Cas) signaling
738 protein functions with integrins to specify axon guidance during development.
739 Development 134:2337–2347. https://doi.org/10.1242/dev.004242

740 Huynh-Do U, Stein E, Lane AA, et al (1999) Surface densities of ephrin-B1 determine EphB1-
741 coupled activation of cell attachment through alphavbeta3 and alpha5beta1 integrins.
742 EMBO J 18:2165–2173. https://doi.org/10.1093/emboj/18.8.2165

743 Hynes RO (1992) Integrins: versatility, modulation, and signaling in cell adhesion. Cell 69:11–25.
744 https://doi.org/10.1016/0092-8674(92)90115-s

745 Islam SM, Shinmyo Y, Okafuji T, et al (2009) Draxin, a repulsive guidance protein for spinal cord
746 and forebrain commissures. Science 323:388–393.
747 https://doi.org/10.1126/science.1165187

748 Ito A, Shinmyo Y, Abe T, et al (2010) Tsukushi is required for anterior commissure formation in
749 mouse brain. Biochem Biophys Res Commun 402:813–818.
750 https://doi.org/10.1016/j.bbrc.2010.10.127

751 Jaudon F, Thalhammer A, Cingolani LA (2021) Integrin adhesion in brain assembly: From
752 molecular structure to neuropsychiatric disorders. Eur J Neurosci 53:3831–3850.
753 https://doi.org/10.1111/ejn.14859

754 Jouandet ML, Hartenstein V (1983) Basal telencephalic origins of the anterior commissure of the
755 rat. Exp Brain Res 50:183–192. https://doi.org/10.1007/BF00239182

756 Kanold PO (2009) Subplate neurons: crucial regulators of cortical development and plasticity.
757 Front Neuroanat 3:16. https://doi.org/10.3389/neuro.05.016.2009

758 Kanold PO, Kara P, Reid RC, Shatz CJ (2003) Role of subplate neurons in functional maturation of
759 visual cortical columns. Science 301:521–525. https://doi.org/10.1126/science.1084152

760 Kanold PO, Luhmann HJ (2010) The subplate and early cortical circuits. Annu Rev Neurosci
761 33:23–48. https://doi.org/10.1146/annurev-neuro-060909-153244

762 Kerstein PC, Nichol RH, Gomez TM (2015) Mechanochemical regulation of growth cone motility.
763 Front Cell Neurosci 9:244. https://doi.org/10.3389/fncel.2015.00244

764 Klingler E, Martin P-M, Garcia M, et al (2015) The cytoskeleton-associated protein SCHIP1 is
765 involved in axon guidance, and is required for piriform cortex and anterior commissure
766 development. Development 142:2026–2036. https://doi.org/10.1242/dev.119248

767 Kolodkin AL, Tessier-Lavigne M (2011) Mechanisms and molecules of neuronal wiring: a primer.
768 Cold Spring Harb Perspect Biol 3:a001727. https://doi.org/10.1101/cshperspect.a001727

769 Kwon YT, Tsai LH, Crandall JE (1999) Callosal axon guidance defects in p35(-/-) mice. J Comp
770 Neurol 415:218–229. https://doi.org/10.1002/(sici)1096-
771 9861(19991213)415:2<218::aid-cne6>3.0.co;2-f

772 Lefcort F, Bentley D (1987) Pathfinding by pioneer neurons in isolated, opened and mesoderm-
773 free limb buds of embryonic grasshoppers. Dev Biol 119:466–480.
774 https://doi.org/10.1016/0012-1606(87)90050-9

775 Lent R, Uziel D, Baudrimont M, Fallet C (2005) Cellular and molecular tunnels surrounding the
776 forebrain commissures of human fetuses. J Comp Neurol 483:375–382.
777 https://doi.org/10.1002/cne.20427

778 Lilja J, Ivaska J (2018) Integrin activity in neuronal connectivity. J Cell Sci 131:jcs212803.
779 https://doi.org/10.1242/jcs.212803

780 Liu G, Li W, Gao X, et al (2007) p130CAS is required for netrin signaling and commissural axon
781 guidance. J Neurosci 27:957–968. https://doi.org/10.1523/JNEUROSCI.4616-06.2007

782 López-Bendito G (2018) Development of the Thalamocortical Interactions: Past, Present and
783 Future. Neuroscience 385:67–74. https://doi.org/10.1016/j.neuroscience.2018.06.020

784 López-Bendito G, Cautinat A, Sánchez JA, et al (2006) Tangential neuronal migration controls
785 axon guidance: a role for neuregulin-1 in thalamocortical axon navigation. Cell 125:127–
786 142. https://doi.org/10.1016/j.cell.2006.01.042

787 López-Bendito G, Flames N, Ma L, et al (2007) Robo1 and Robo2 cooperate to control the
788 guidance of major axonal tracts in the mammalian forebrain. J Neurosci 27:3395–3407.
789 https://doi.org/10.1523/JNEUROSCI.4605-06.2007

790 López-Bendito G, Molnár Z (2003) Thalamocortical development: how are we going to get
791 there? Nat Rev Neurosci 4:276–289. https://doi.org/10.1038/nrn1075

792 Machiyama H, Hirata H, Loh XK, et al (2014) Displacement of p130Cas from focal adhesions links
793 actomyosin contraction to cell migration. J Cell Sci 127:3440–3450.
794 https://doi.org/10.1242/jcs.143438

795 Madisen L, Zwingman TA, Sunkin SM, et al (2010) A robust and high-throughput Cre reporting
796 and characterization system for the whole mouse brain. Nat Neurosci 13:133–140.
797 https://doi.org/10.1038/nn.2467

798 Marcus RC, Blazeski R, Godement P, Mason CA (1995) Retinal axon divergence in the optic
799 chiasm: uncrossed axons diverge from crossed axons within a midline glial specialization.
800 J Neurosci 15:3716–3729. https://doi.org/10.1523/JNEUROSCI.15-05-03716.1995

801 Martin-Lopez E, Meller SJ, Greer CA (2018) Development of piriform cortex interhemispheric
802 connections via the anterior commissure: progressive and regressive strategies. Brain
803 Struct Funct 223:4067–4085. https://doi.org/10.1007/s00429-018-1741-y

804 McCarty JH, Lacy-Hulbert A, Charest A, et al (2005) Selective ablation of alphav integrins in the
805 central nervous system leads to cerebral hemorrhage, seizures, axonal degeneration and
806 premature death. Development 132:165–176. https://doi.org/10.1242/dev.01551

807 McConnell SK, Ghosh A, Shatz CJ (1989) Subplate neurons pioneer the first axon pathway from
808 the cerebral cortex. Science 245:978–982. https://doi.org/10.1126/science.2475909

809 Milner R, Campbell IL (2002) The integrin family of cell adhesion molecules has multiple
810 functions within the CNS. J Neurosci Res 69:286–291. https://doi.org/10.1002/jnr.10321

811 Molnár Z, Adams R, Blakemore C (1998a) Mechanisms underlying the early establishment of
812 thalamocortical connections in the rat. J Neurosci 18:5723–5745.
813 https://doi.org/10.1523/JNEUROSCI.18-15-05723.1998

814 Molnár Z, Adams R, Goffinet AM, Blakemore C (1998b) The role of the first postmitotic cortical
815 cells in the development of thalamocortical innervation in the reeler mouse. J Neurosci
816 18:5746–5765. https://doi.org/10.1523/JNEUROSCI.18-15-05746.1998

817 Molnár Z, Garel S, López-Bendito G, et al (2012) Mechanisms controlling the guidance of
818 thalamocortical axons through the embryonic forebrain. Eur J Neurosci 35:1573–1585.
819 https://doi.org/10.1111/j.1460-9568.2012.08119.x

820 Molnár Z, Kwan KY (2024) Development and Evolution of Thalamocortical Connectivity. Cold
821 Spring Harb Perspect Biol 16:a041503. https://doi.org/10.1101/cshperspect.a041503

822 Monko T, Rebertus J, Stolley J, et al (2022) Thalamocortical axons regulate neurogenesis and
823 laminar fates in the early sensory cortex. Proc Natl Acad Sci U S A 119:e2201355119.
824 https://doi.org/10.1073/pnas.2201355119

825 Moos M, Tacke R, Scherer H, et al (1988) Neural adhesion molecule L1 as a member of the
826 immunoglobulin superfamily with binding domains similar to fibronectin. Nature
827 334:701–703. https://doi.org/10.1038/334701a0

828 Moreland T, Poulain FE (2022) To Stick or Not to Stick: The Multiple Roles of Cell Adhesion
829 Molecules in Neural Circuit Assembly. Front Neurosci 16:889155.
830 https://doi.org/10.3389/fnins.2022.889155

831 Munakata H, Nakamura Y, Matsumoto-Miyai K, et al (2003) Distribution and densitometry
832 mapping of L1-CAM immunoreactivity in the adult mouse brain--light microscopic
833 observation. BMC Neurosci 4:7. https://doi.org/10.1186/1471-2202-4-7

834 Myers JP, Santiago-Medina M, Gomez TM (2011) Regulation of axonal outgrowth and
835 pathfinding by integrin-ECM interactions. Dev Neurobiol 71:901–923.
836 https://doi.org/10.1002/dneu.20931

837 Ohtaka-Maruyama C (2020) Subplate Neurons as an Organizer of Mammalian Neocortical
838 Development. Front Neuroanat 14:8. https://doi.org/10.3389/fnana.2020.00008

839 O'Leary DD, Schlaggar BL, Tuttle R (1994) Specification of neocortical areas and thalamocortical
840 connections. Annu Rev Neurosci 17:419–439.
841 https://doi.org/10.1146/annurev.ne.17.030194.002223

842 Pires-Neto MA, Braga-De-Souza S, Lent R (1998) Molecular tunnels and boundaries for growing
843 axons in the anterior commissure of hamster embryos. J Comp Neurol 399:176–188.
844 https://doi.org/10.1002/(sici)1096-9861(19980921)399:2<176::aid-cne3>3.0.co;2-y

845 Qu Y, Huang Y, Feng J, et al (2014) Genetic evidence that Celsr3 and Celsr2, together with Fzd3,
846 regulate forebrain wiring in a Vangl-independent manner. Proc Natl Acad Sci U S A
847 111:E2996-3004. https://doi.org/10.1073/pnas.1402105111

848 Renaudin A, Lehmann M, Girault J, McKerracher L (1999) Organization of point contacts in
849 neuronal growth cones. J Neurosci Res 55:458–471. https://doi.org/10.1002/(SICI)1097-
850 4547(19990215)55:4<458::AID-JNR6>3.0.CO;2-D

851 Riccomagno MM, Sun LO, Brady CM, et al (2014) Cas adaptor proteins organize the retinal
852 ganglion cell layer downstream of integrin signaling. Neuron 81:779–786.
853 https://doi.org/10.1016/j.neuron.2014.01.036

854 Robichaux MA, Chenaux G, Ho H-YH, et al (2016) EphB1 and EphB2 intracellular domains
855 regulate the formation of the corpus callosum and anterior commissure. Dev Neurobiol
856 76:405–420. https://doi.org/10.1002/dneu.22323

857 Ruest PJ, Shin NY, Polte TR, et al (2001) Mechanisms of CAS substrate domain tyrosine
858 phosphorylation by FAK and Src. Mol Cell Biol 21:7641–7652.
859 https://doi.org/10.1128/MCB.21.22.7641-7652.2001

860 Sahay A, Molliver ME, Ginty DD, Kolodkin AL (2003) Semaphorin 3F is critical for development of
861 limbic system circuitry and is required in neurons for selective CNS axon guidance
862 events. J Neurosci 23:6671–6680. https://doi.org/10.1523/JNEUROSCI.23-17-
863 06671.2003

864 Schmid RS, Anton ES (2003) Role of integrins in the development of the cerebral cortex. Cereb
865 Cortex 13:219–224. https://doi.org/10.1093/cercor/13.3.219

866 Schwartz MA (2001) Integrin signaling revisited. Trends Cell Biol 11:466–470.
867 https://doi.org/10.1016/s0962-8924(01)02152-3

868 Seo S, Asai T, Saito T, et al (2005) Crk-associated substrate lymphocyte type is required for
869 lymphocyte trafficking and marginal zone B cell maintenance. J Immunol 175:3492–
870 3501. https://doi.org/10.4049/jimmunol.175.6.3492

871 Serafini T, Colamarino SA, Leonardo ED, et al (1996) Netrin-1 is required for commissural axon
872 guidance in the developing vertebrate nervous system. Cell 87:1001–1014.
873 https://doi.org/10.1016/s0092-8674(00)81795-x

874 Shen Y, Mani S, Donovan SL, et al (2002) Growth-associated protein-43 is required for
875 commissural axon guidance in the developing vertebrate nervous system. J Neurosci
876 22:239–247. https://doi.org/10.1523/JNEUROSCI.22-01-00239.2002

877 Shu T, Li Y, Keller A, Richards LJ (2003) The glial sling is a migratory population of developing
878 neurons. Development 130:2929–2937. https://doi.org/10.1242/dev.00514

879 Shu T, Richards LJ (2001) Cortical axon guidance by the glial wedge during the development of
880 the corpus callosum. J Neurosci 21:2749–2758. https://doi.org/10.1523/JNEUROSCI.21-
881 08-02749.2001

882 Silver J, Edwards MA, Levitt P (1993) Immunocytochemical demonstration of early appearing
883 astroglial structures that form boundaries and pathways along axon tracts in the fetal
884 brain. J Comp Neurol 328:415–436. https://doi.org/10.1002/cne.903280308

885 Spead O, Poulain FE (2020) Trans-Axonal Signaling in Neural Circuit Wiring. Int J Mol Sci 21:5170.
886 https://doi.org/10.3390/ijms21145170

887 Squarzoni P, Thion MS, Garel S (2015) Neuronal and microglial regulators of cortical wiring:
888 usual and novel guideposts. Front Neurosci 9:248.
889 https://doi.org/10.3389/fnins.2015.00248

890 Stein E, Huynh-Do U, Lane AA, et al (1998a) Nck recruitment to Eph receptor, EphB1/ELK,
891 couples ligand activation to c-Jun kinase. J Biol Chem 273:1303–1308.
892 https://doi.org/10.1074/jbc.273.3.1303

893 Stein E, Lane AA, Cerretti DP, et al (1998b) Eph receptors discriminate specific ligand oligomers
894 to determine alternative signaling complexes, attachment, and assembly responses.
895 Genes Dev 12:667–678. https://doi.org/10.1101/gad.12.5.667

896 Suh LH, Oster SF, Soehrman SS, et al (2004) L1/Laminin modulation of growth cone response to
897 EphB triggers growth pauses and regulates the microtubule destabilizing protein SCG10.
898 J Neurosci 24:1976–1986. https://doi.org/10.1523/JNEUROSCI.1670-03.2004

899 Suto F, Ito K, Uemura M, et al (2005) Plexin-a4 mediates axon-repulsive activities of both
900 secreted and transmembrane semaphorins and plays roles in nerve fiber guidance. J
901 Neurosci 25:3628–3637. https://doi.org/10.1523/JNEUROSCI.4480-04.2005

902 Takada Y, Ye X, Simon S (2007) The integrins. Genome Biol 8:215. https://doi.org/10.1186/gb-
903 2007-8-5-215

904 Tessier-Lavigne M, Goodman CS (1996) The molecular biology of axon guidance. Science
905 274:1123–1133. https://doi.org/10.1126/science.274.5290.1123

906 Tissir F, Bar I, Jossin Y, et al (2005) Protocadherin Celsr3 is crucial in axonal tract development.
907 Nat Neurosci 8:451–457. https://doi.org/10.1038/nn1428

908 Tole S, Gutin G, Bhatnagar L, et al (2006) Development of midline cell types and commissural
909 axon tracts requires Fgfr1 in the cerebrum. Dev Biol 289:141–151.
910 https://doi.org/10.1016/j.ydbio.2005.10.020

911 Tolner EA, Sheikh A, Yukin AY, et al (2012) Subplate neurons promote spindle bursts and
912 thalamocortical patterning in the neonatal rat somatosensory cortex. J Neurosci 32:692–
913 702. https://doi.org/10.1523/JNEUROSCI.1538-11.2012

914 Tronche F, Kellendonk C, Kretz O, et al (1999) Disruption of the glucocorticoid receptor gene in
915 the nervous system results in reduced anxiety. Nat Genet 23:99–103.
916 https://doi.org/10.1038/12703

917 Vahedi-Hunter TA, Estep JA, Rosette KA, et al (2018) Cas Adaptor Proteins Coordinate Sensory
918 Axon Fasciculation. Sci Rep 8:5996. https://doi.org/10.1038/s41598-018-24261-x

919 Vanderhaeghen P, Polleux F (2004) Developmental mechanisms patterning thalamocortical
920 projections: intrinsic, extrinsic and in between. Trends Neurosci 27:384–391.
921 https://doi.org/10.1016/j.tins.2004.05.009

922 Viswanathan S, Bandyopadhyay S, Kao JPY, Kanold PO (2012) Changing microcircuits in the
923 subplate of the developing cortex. J Neurosci 32:1589–1601.
924 https://doi.org/10.1523/JNEUROSCI.4748-11.2012

925 Vuori K, Hirai H, Aizawa S, Ruoslahti E (1996) Introduction of p130cas signaling complex
926 formation upon integrin-mediated cell adhesion: a role for Src family kinases. Mol Cell
927 Biol 16:2606–2613. https://doi.org/10.1128/MCB.16.6.2606

928 Wang JF, Park IW, Groopman JE (2000) Stromal cell-derived factor-1alpha stimulates tyrosine
929 phosphorylation of multiple focal adhesion proteins and induces migration of
930 hematopoietic progenitor cells: roles of phosphoinositide-3 kinase and protein kinase C.
931 Blood 95:2505–2513

932 Wang L, Marquardt T (2013) What axons tell each other: axon-axon signaling in nerve and circuit
933 assembly. Curr Opin Neurobiol 23:974–982. https://doi.org/10.1016/j.conb.2013.08.004

934 Wong W, Estep JA, Treptow AM, et al (2023) An adhesion signaling axis involving Dystroglycan,
935 β1-Integrin, and Cas adaptor proteins regulates the establishment of the cortical glial
936 scaffold. PLoS Biol 21:e3002212. https://doi.org/10.1371/journal.pbio.3002212

937 Wu S-X, Goebbels S, Nakamura K, et al (2005) Pyramidal neurons of upper cortical layers
938 generated by NEX-positive progenitor cells in the subventricular zone. Proc Natl Acad Sci
939 U S A 102:17172–17177. https://doi.org/10.1073/pnas.0508560102

940 Xu N-J, Henkemeyer M (2009) Ephrin-B3 reverse signaling through Grb4 and cytoskeletal
941 regulators mediates axon pruning. Nat Neurosci 12:268–276.
942 https://doi.org/10.1038/nn.2254

943 Yan L, Cui Z (2023) Integrin β1 and the Repair after Nervous System Injury. Eur Neurol 86:2–12.
944 https://doi.org/10.1159/000526690

945

946

947 **Figure Legends**

948 **Figure 1. *p130Cas* is expressed in the cortical white matter.** (**A-E''**) Detection of EGFP (green)
949 expression of *p130Cas-EGFP-BAC* transgenic mice co-immunolabeled with the axonal marker
950 NCAM-L1 (red) at E14.5 (**A-A''**), E16.5 (**B-B''**), and P0 (**C-C''**). Analysis reveals strong *p130Cas*
951 promoter activity during the formation of cortical white matter tracts. Robust EGFP expression
952 is observed in the External Capsule (EC) (**A, B, C**, white asterisk) and Anterior Commissure (AC) (
953 **A, B, C**, white arrowheads). High resolution images at P0 show EGFP (**D', E'**) and NCAM-L1 (**D'',**
954 **E''**) expression at the pallial-subpallial boundary (**D**, dotted line) and the cortical plate (**E**). Scale
955 bar = 250µm.

956

957 **Figure 2. *Cas TcKO* mutants display errors in cortical and thalamocortical connections. (A-B'')**
958 Immunohistological analysis of major cortical tracts using the axonal marker NCAM-L1 (green) in
959 *Nes-Cre;TcKO* mutant and control neonates (P0). Two major defasciculation phenotypes are
960 present in *Nes-Cre;TcKO* mice: 1) efferents originating in the cortex fail to fasciculate properly in
961 the pAC tract and erroneously project into the subpallium (**B'**), and 2) thalamocortical
962 connections meant to innervate layer IV mis-project to the subpial boundary, forming large
963 Cortical Bundles (**B''**). Each of these phenotypes is fully penetrant in *Nes-Cre;TcKO* mutants. (**C-**
964 **H**) The origin of mis-projecting axons is confirmed via anterograde lipophilic tracing
965 experiments. DiA crystals placed into the S2 cortex label ventrally defasciculating AC axons (**D**,
966 arrowheads) but not Cortical Bundles (**F**) in *Nes-Cre;TcKO* mutants. DiI crystals placed in the
967 laterodorsal thalamus label Cortical Bundles (**H**, white asterisks). (**I**) Quantification of the

968 number of stray axons in the subpallial area. Unpaired *t*-test, ***p < 0.001, n = 7 for *Nes-*
969 *Cre;TcKO,* n = 10 for controls. (**J**) Quantification of the number of Cortical Bundles. Unpaired *t-*
970 test, ****p < 0.0001, n = 8 for *Nes-Cre;TcKO,* n = 7 for controls. Values provided are mean ±
971 SEM. Scale bar = 250µm.

972

973 **Figure 3. Developmental progression of white matter defects in *Nes-Cre;TcKO* mutants.** (**A-F''**)
974 Immunohistochemistry for the axonal marker NCAM-L1 (green) in *Nes-Cre;TcKO* mutants and
975 control mice at E14.5 (**A-B''**), E16.5, (**C-D''**), and E18.5 (**E-F''**). Analysis reveals different
976 developmental timelines for each defasciculation phenotype. The EC-AC tract begin developing
977 at E14.5 in control (**A'**) and *Nes-Cre;TcKO* mice (**B'**). *Nes-Cre;TcKO* mice display no AC
978 defasciculation errors until E18.5 (**F'**, white arrowhead). Cortical Bundles are apparent at E14.5
979 in *Nes-Cre;TcKO* mutants (**B''**, white asterisks) and worsen in severity as development continues
980 (**D''** and **F''**, white asterisks). (**G**) Quantification of the average number of stray axons in the
981 subpallial area at E18.5. Unpaired *t*-test, **p < 0.01, n = 5 for *Nes-Cre;TcKO,* n = 4 for controls.
982 (**H**) Quantification of the average number of Cortical Bundles at E14.6, E16.5 and E18.5. Two-
983 way ANOVA, p < 0.0001; Tukey HSD post hoc test, ****p < 0.0001 E14.5 *Nes-Cre;TcKO* versus
984 control, E16.5 *Nes-Cre;TcKO* versus control, E18.5 *Nes-Cre;TcKO* versus control, E14.5 *Nes-*
985 *Cre;TcKO* versus E18.5 *Nes-Cre;TcKO*, E16.5 *Nes-Cre;TcKO* versus E18.5 *Nes-Cre;TcKO*; ns E14.5
986 *Nes-Cre;TcKO* vs E16.5 *Nes-Cre;TcKO*; E14.5: n = 4 for *Nes-Cre;TcKO,* n = 4 for controls; E16.5: n =
987 8 for *Nes-Cre;TcKO,* n = 12 for controls; E18.5: n = 5 for *Nes-Cre;TcKO,* n = 4 for controls). Values
988 provided are mean ± SEM. Scale bar = 250µm.

989 **Figure 4. Neuronal-autonomous and non-neuronal autonomous roles for *Cas* genes in white**
990 **matter tract fasciculation.** (**A-H''**) Immunohistochemistry for the axonal marker NCAM-L1
991 (green) in *Emx1-Cre;TcKO* and *Nex-Cre;TcKO* neonates. Analysis reveals both classes of
992 conditional knockouts present the AC defasciculation phenotype (**B'** and **H'**, white arrowheads),
993 indicating this phenotype is neuronal-autonomous. This phenotype fully penetrant in *Emx1-*
994 *Cre;TcKO* and *Nex-Cre;TcKO* mutants. Similar to *Nes-Cre;TcKO* mutants (**Figure 2**), defasciculating
995 axons in the subpallial area of *Emx1-Cre;TcKO* and *Nex-Cre;TcKO* mutants are cortical in origin as
996 revealed by anterograde DiA tracing from crystal placement in the S2 cortex (**D** and **J**, white
997 arrowheads). In contrast, only *Emx1-Cre;TcKO* mutants display the Cortical Bundle phenotype
998 (**B''**, white asterisks). Cortical Bundles are confirmed to be TCA projections by anterograde
999 labeling from DiI crystals placed in the laterodorsal thalamus (**F**, white asterisks). The absence of
1000 the Cortical Bundle phenotype in *Nex-Cre;TcKO* mutants (**H''** and **L**) indicates the role of *Cas*
1001 genes during TCA fasciculation and projection is non-neuronal autonomous. (**M**) Quantification
1002 of the number of stray axons in the subpallial area in *Emx1-Cre;TcKO* mutants and controls.
1003 Unpaired *t*-test, ****$p < 0.0001$, n = 8 for *Emx1-Cre;TcKO,* n = 10 for controls. (**N**) Quantification
1004 of the number of Cortical Bundles in *Emx1-Cre;TcKO* mutants and controls. Unpaired *t*-test,
1005 ****$p < 0.0001$, n = 8 for *Emx1-Cre;TcKO,* n = 10 for controls (**O**) Quantification of the number of
1006 stray axons in the subpallial area of *Nex-Cre;TcKO* mutants and controls. Unpaired *t*-test, ****p
1007 < 0.0001, n = 7 for *Nex-Cre;TcKO,* n = 5 for controls. Values provided are mean ± SEM. Scale bar =
1008 250µm.

1009

1010 **Figure 5. Genetic labeling confirms cortical origins of AC defasciculating axons in *Cas TcKO***
1011 **mutants.** (**A-H''**) Immunohistochemistry for NCAM-L1 (green) and the tdTomato fluorescent
1012 Cre-dependent reporter (red). Analysis reveals extensive co-labeling in defasciculating AC axon
1013 bundles in both *Emx1-Cre;Ai14*$^{+/-}$*;TcKO* (**C-D''**) and *Nex-Cre;Ai14*$^{+/-}$*;TcKO* (**G-H''**) mutants. In both
1014 classes of conditional mutants, tdTomato+ defasciculating axons appear to interpolate with
1015 diffuse NCAM-L1+ processes that occupy the subpallium (**D' vs D''** and **H' vs H''**, white
1016 arrowheads). No tdTomato+ processes may be seen invading the subpallium in *Emx1-Cre;Ai14*$^{+/-}$
1017 *;CasL*$^{+/-}$*;Sin*$^{+/-}$*;p130Cas*$^{+/+}$ controls (**A-B''**) and *Nex-Cre;Ai14*$^{+/-}$*;CasL*$^{+/-}$*;Sin*$^{+/-}$*;p130Cas*$^{+/+}$ (**E-F''**)
1018 controls. (**I**) Quantification of the number of stray axons in the subpallial area of *Emx1-*
1019 *Cre;Ai14*$^{+/-}$*;TcKO* mutants and controls. Unpaired *t*-test, ****$p < 0.0001$, n = 3 for *Emx1-*
1020 *Cre;Ai14*$^{+/-}$*;TcKO*, n = 3 for controls. (**J**) Quantification of the number of stray axons in the
1021 subpallial area of *Nex-Cre;Ai14*$^{+/-}$*;TcKO* mutants and controls. Unpaired *t*-test, *$p < 0.05$, n = 4 for
1022 *Nex-Cre;Ai14*$^{+/-}$*;TcKO,* n = 3 for controls. Values provided are mean ± SEM. Scale bar = 250µm.

1023

1024 **Figure 6. *Itgb1* mutants phenocopy the non-neuronal autonomous TCA tract defects observed**
1025 **in *Cas TcKO* mutants. (A-D'')** Immunohistological analysis of NCAM-L1 (green) in *Emx1-*
1026 *Cre;Itgb1*$^{fl/fl}$ and *Nex-Cre;Itgb1*$^{fl/fl}$ neonates. Neither class of conditional mutant phenocopies the
1027 AC defasciculation defects observed in *Cas TcKO* mutants (**B'** and **D'**), suggesting that β1-integrin
1028 is dispensable for AC tract fasciculation. Only *Emx1-Cre;Itgb1*$^{fl/fl}$ mutants phenocopy the Cortical
1029 Bundle phenotype observed in *Cas TcKO* mutants (**B''**, white asterisks), indicating a similar non-
1030 neuronal autonomous role of β1-integrin during TCA projection. (**E**) Quantification of the
1031 number of Cortical Bundles in *Emx1-Cre;Itgb1*$^{fl/fl}$ mutants and controls. Unpaired *t*-test, ****p <

1032 0.0001, n = 6 for *Emx1-Cre;Itgb1*$^{fl/fl}$, n = 5 for controls. Values provided are mean ± SEM. Scale

1033 bar = 250µm.

1034 **Figure 7. Non-neuronal autonomous phenotypes in E16.5 *Itgb1* and *Cas TcKO* mutants**

1035 **correlate with displaced subplate cells. (A-H'')** Immunohistochemistry of Tbr1 (red) and NCAM-

1036 L1 (green) in E16.5 *Emx1-Cre;TcKO* and *Emx1-Cre;Itgb1*$^{fl/fl}$ mutants. Analysis reveals severe

1037 cortical dysplasia associated with Cortical Bundles. In both classes of conditional mutants, Tbr1+

1038 deep layer/subplate cells are displaced to more superficial layers (**D'** and **H'**, white asterisks).

1039 Cortical Bundles correlate with superficially displaced Tbr1+ deep layer/subplate cells (**D''** and

1040 **H''**, white asterisks). Scale bar = 250µm.

1041

1042 **Figure 8. Non-neuronal autonomous phenotypes in P0 *Itgb1* and *Cas TcKO* neonate mutants**

1043 **correlate with displaced subplate cells. (A-H'')** Immunohistological analysis of Tbr1 (red) and

1044 NCAM-L1 (green) in P0 *Emx1-Cre;TcKO* and *Emx1-Cre;Itgb1*$^{fl/fl}$ mutants. Severe cortical dysplasia

1045 is associated with Cortical Bundles. In both classes of conditional mutants, Tbr1+ deep

1046 layer/subplate cells are displaced to more superficial positions (**D'** and **H'**, white asterisks).

1047 Cortical Bundles correlate with superficially displaced Tbr1+ deep layer/subplate cells (**D''** and

1048 **H''**, white asterisks). Scale bar = 250µm.

1049

1050 **Supplemental Figure 1. Placement of DiA and DiI crystals in *Nes-Cre;TcKO* mutants and**

1051 **controls.** (**A-D'**) DiA and DiI crystal placement in coronal sections from P0 *Nes-Cre;TcKO* and

1052 control mice. DiA crystals were placed into the Somatosensory 2 (S2) region of the cortex (**A, B**),

1053 while DiI crystals were placed into the laterodorsal nucleus of the thalamus (**C, D**). Scale bar =

1054 250µm.

1055

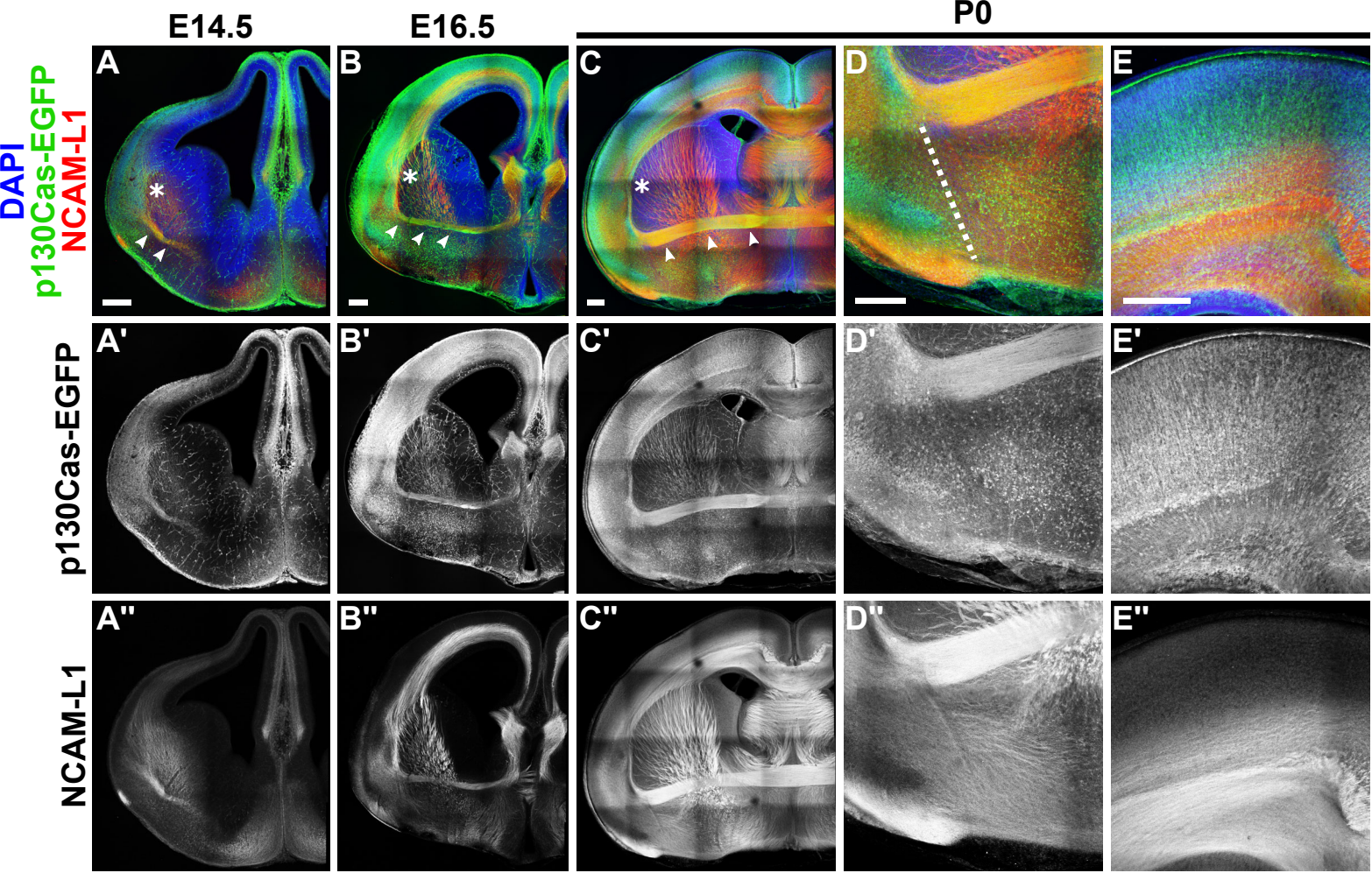
E14.5
E16.5
P0
DAPI
p130Cas-EGFP
NCAM-L1
A
B
C
D
E
A'
B'
C'
D'
E'
A''
B''
C''
D''
E''
p130Cas-EGFP
NCAM-L1

Figure 1

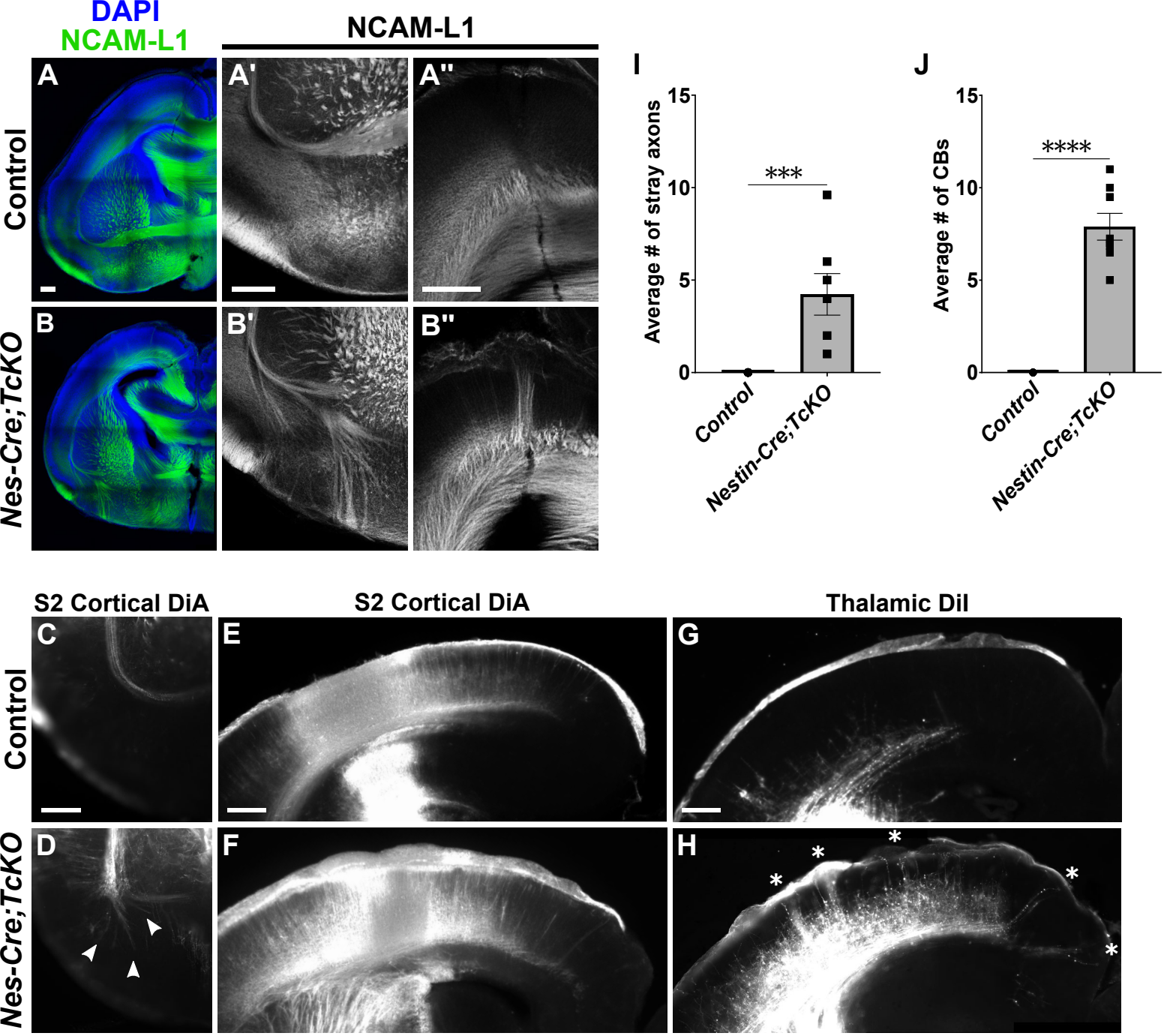
DAPI
NCAM-L1
NCAM-L1
A
A'
A''
B
B'
B''
Control
Nes-Cre;TcKO
I
J
Average # of stray axons
Average # of CBs
15
10
5
0
***
****
Control
Nestin-Cre;TcKO
S2 Cortical DiA
S2 Cortical DiA
Thalamic DiI
C
E
G
D
F
H
Control
Nes-Cre;TcKO

Figure 2

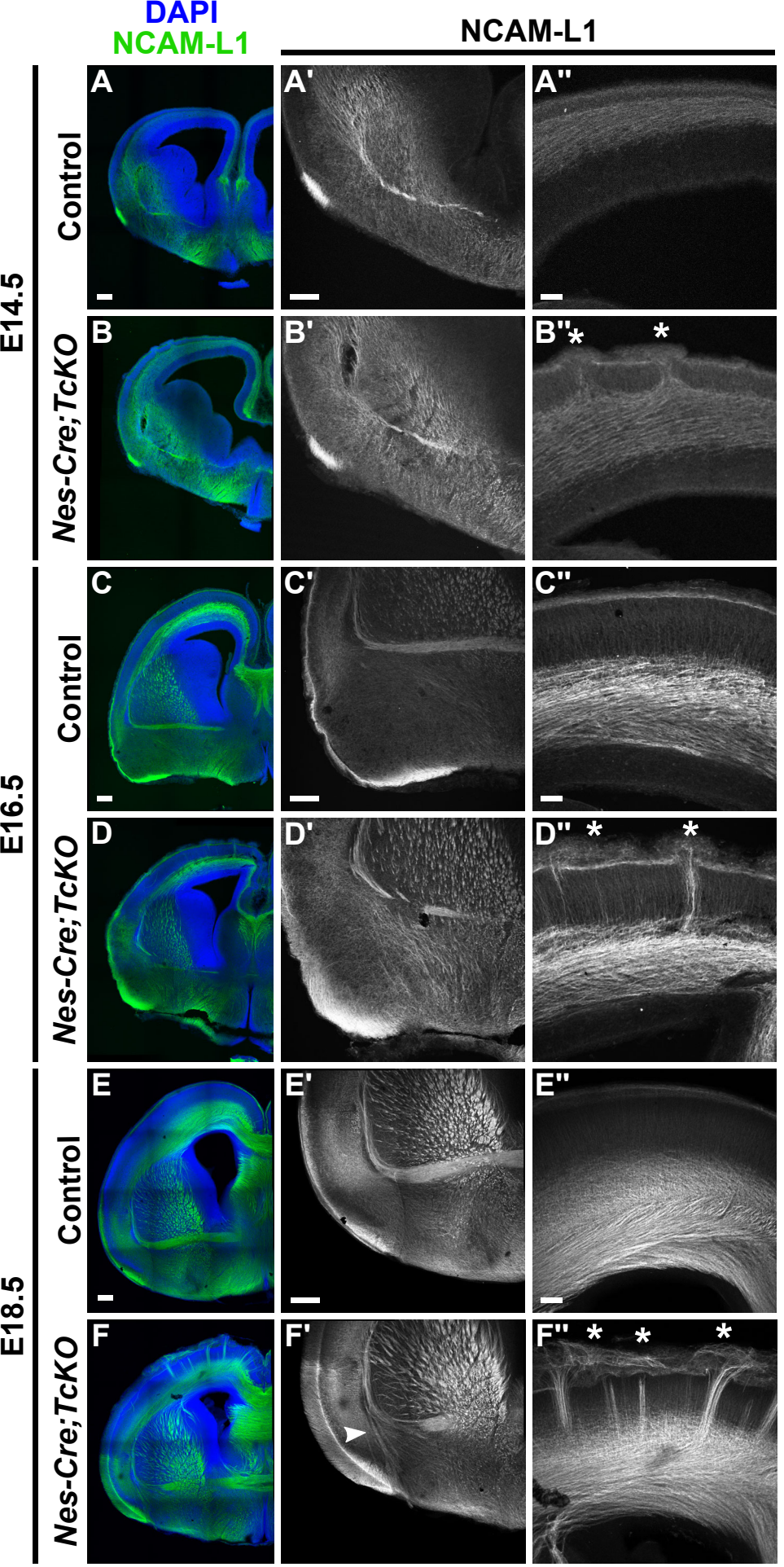
DAPI
NCAM-L1
NCAM-L1
E14.5
E16.5
E18.5
Control
Nes-Cre;TcKO
A
A'
A''
B
B'
B''
C
C'
C''
D
D'
D''
E
E'
E''
F
F'
F''

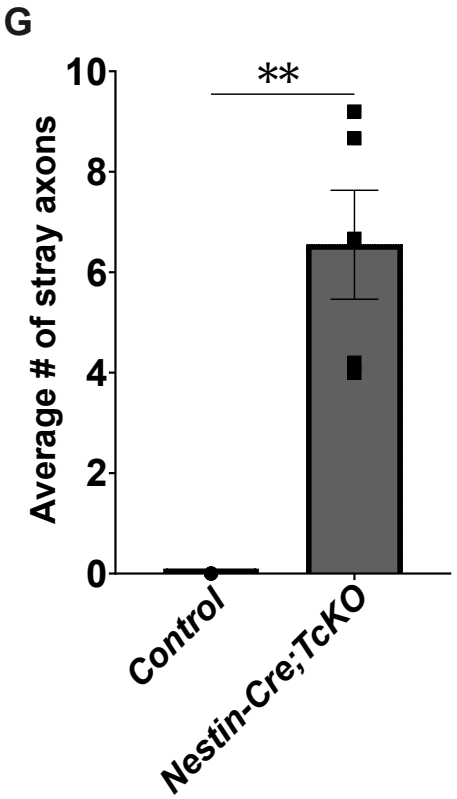
G
Average # of stray axons
10
8
6
4
2
0
**
Control
Nestin-Cre;TcKO

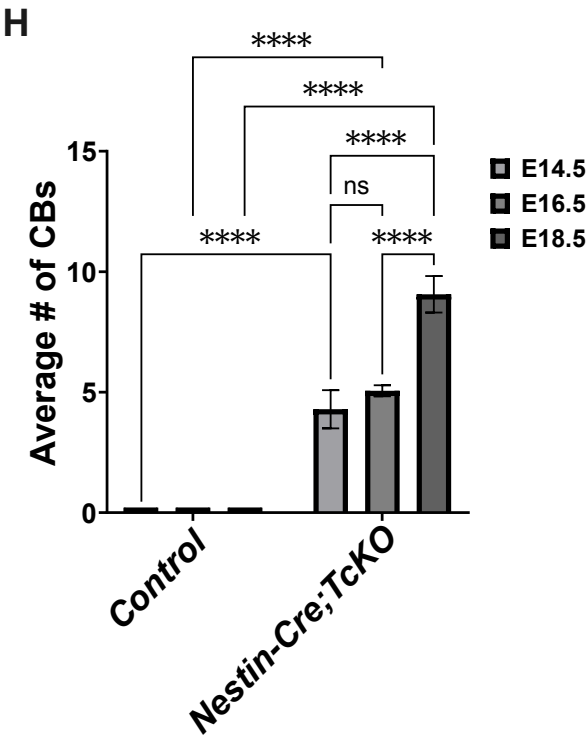
H
Average # of CBs
15
10
5
0
****
****
****
ns
****
****
E14.5
E16.5
E18.5
Control
Nestin-Cre;TcKO

Figure 3

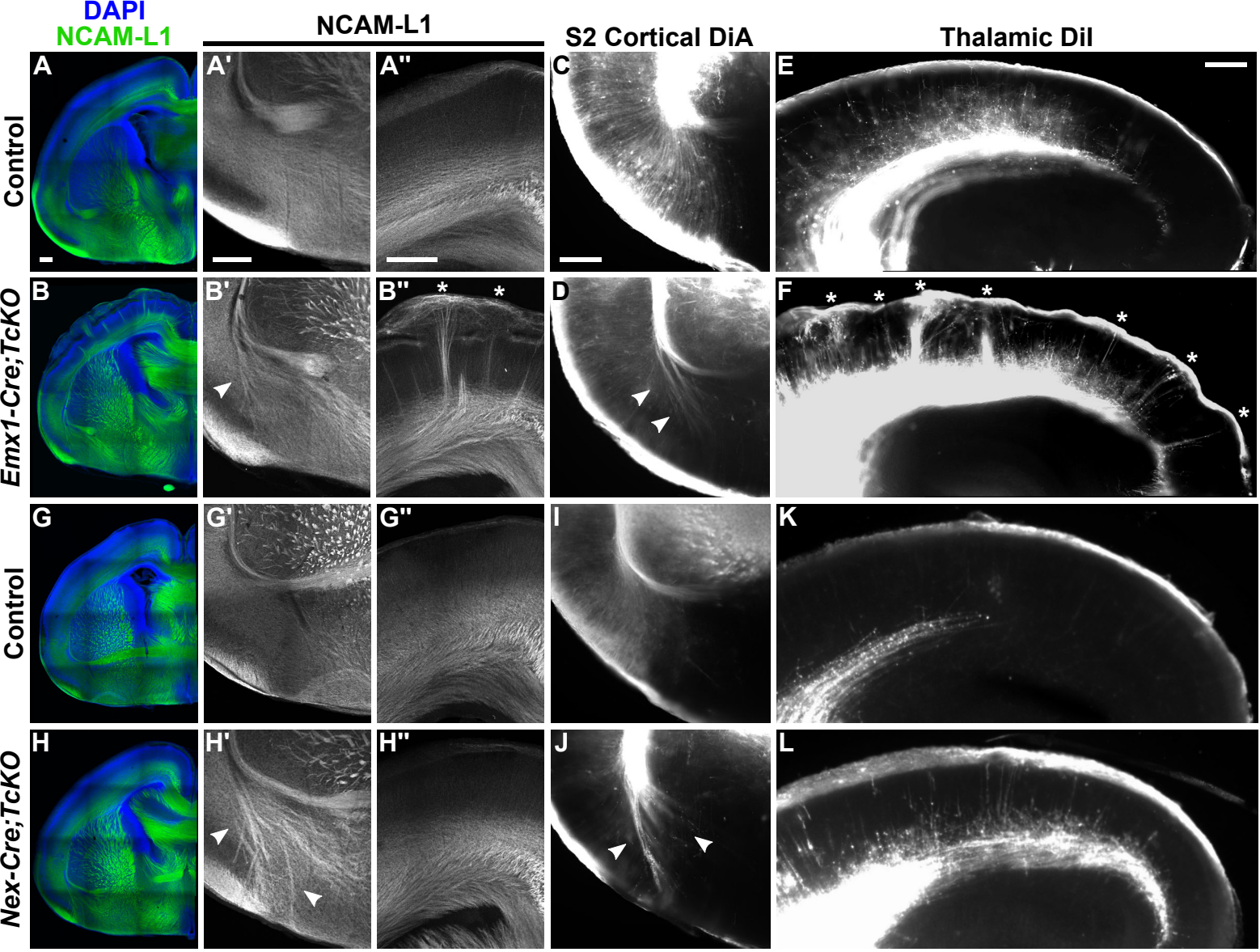
DAPI
NCAM-L1
NCAM-L1
S2 Cortical DiA
Thalamic DiI
Control
Emx1-Cre;TcKO
Control
Nex-Cre;TcKO
A
A'
A''
C
E
B
B'
B''
D
F
G
G'
G''
I
K
H
H'
H''
J
L

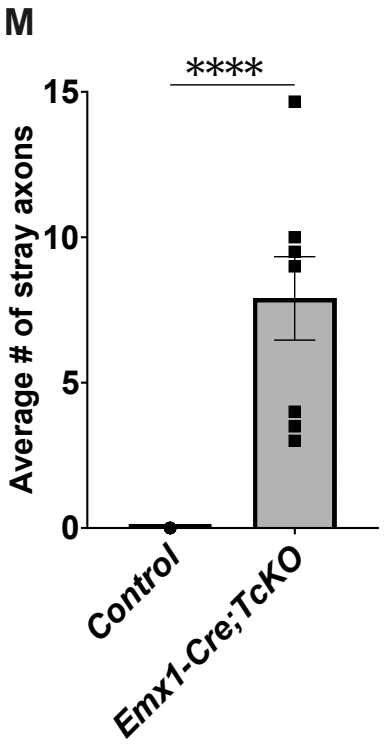
M
****
Average # of stray axons
0
5
10
15
Control
Emx1-Cre;TcKO

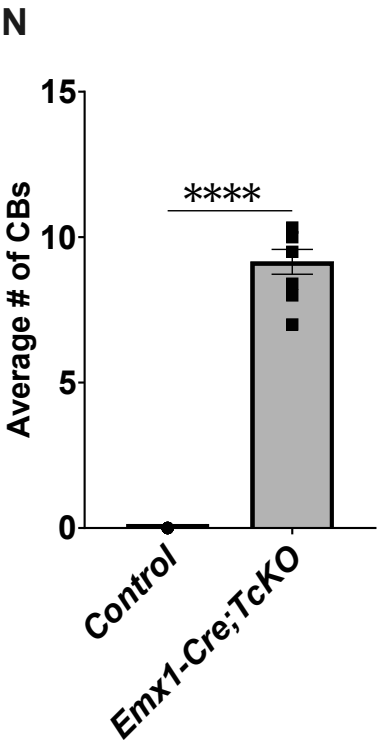
N
****
Average # of CBs
0
5
10
15
Control
Emx1-Cre;TcKO

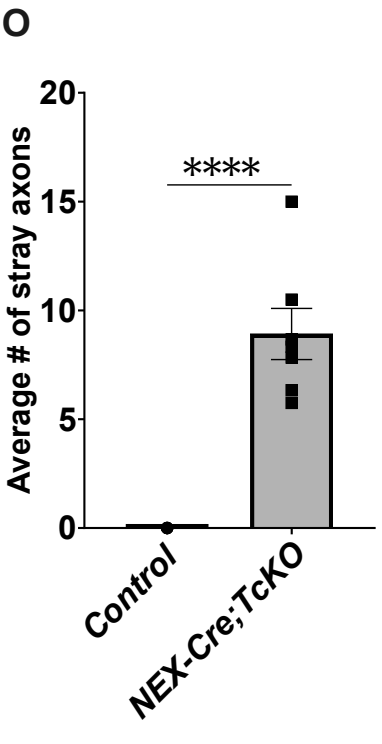
O
****
Average # of stray axons
0
5
10
15
20
Control
NEX-Cre;TcKO

Figure 4

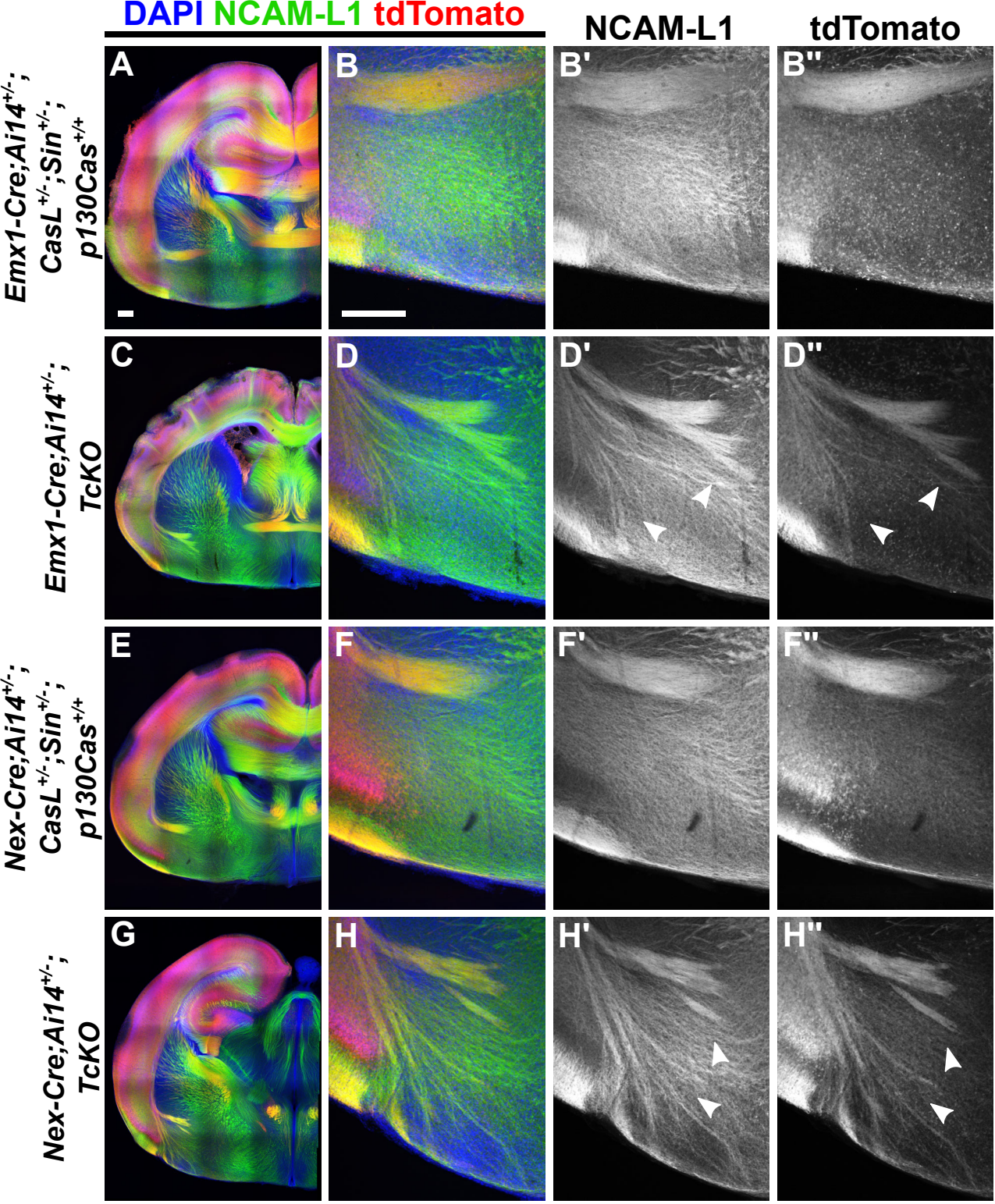
DAPI NCAM-L1 tdTomato
NCAM-L1
tdTomato
Emx1-Cre;Ai14+/-; CasL+/-;Sin+/-; p130Cas+/+
Emx1-Cre;Ai14+/-; TcKO
Nex-Cre;Ai14+/-; CasL+/-;Sin+/-; p130Cas+/+
Nex-Cre;Ai14+/-; TcKO
A
B
B'
B''
C
D
D'
D''
E
F
F'
F''
G
H
H'
H''

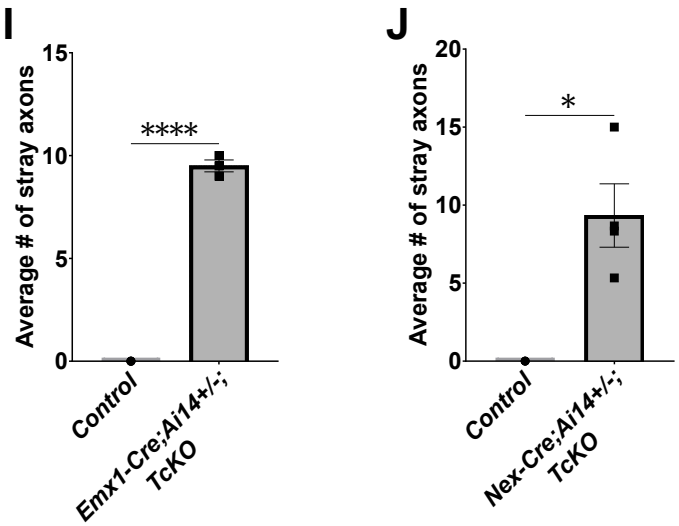
I
Average # of stray axons
15
10
5
0
****
Control
Emx1-Cre;Ai14+/-; TcKO
J
Average # of stray axons
20
15
10
5
0
*
Control
Nex-Cre;Ai14+/-; TcKO

Figure 5

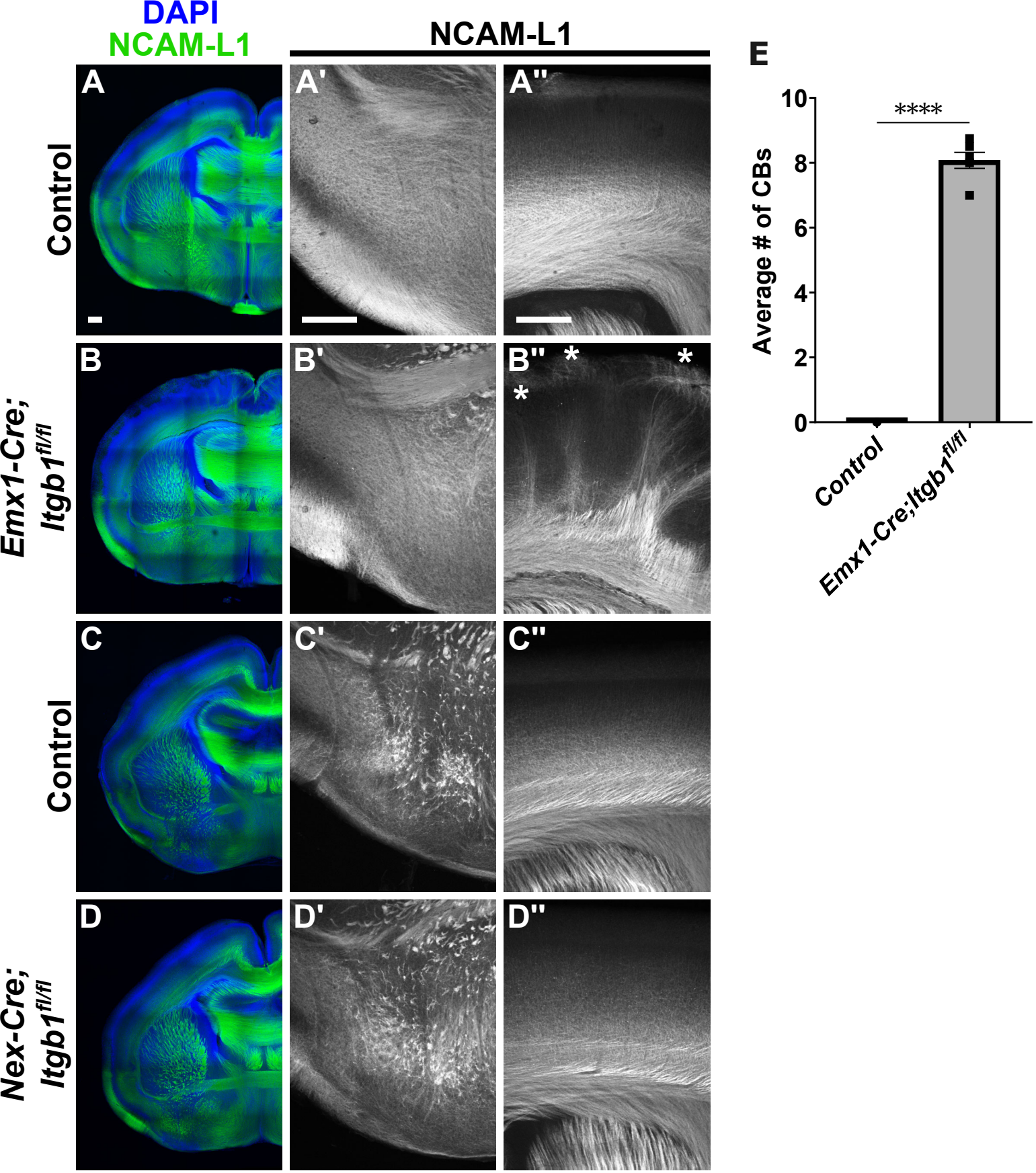
DAPI
NCAM-L1
NCAM-L1
A
A'
A''
B
B'
B''
C
C'
C''
D
D'
D''
Control
Control
Emx1-Cre; Itgb1fl/fl
Nex-Cre; Itgb1fl/fl
E
Average # of CBs
10
8
6
4
2
0
****
Control
Emx1-Cre;Itgb1fl/fl

Figure 6

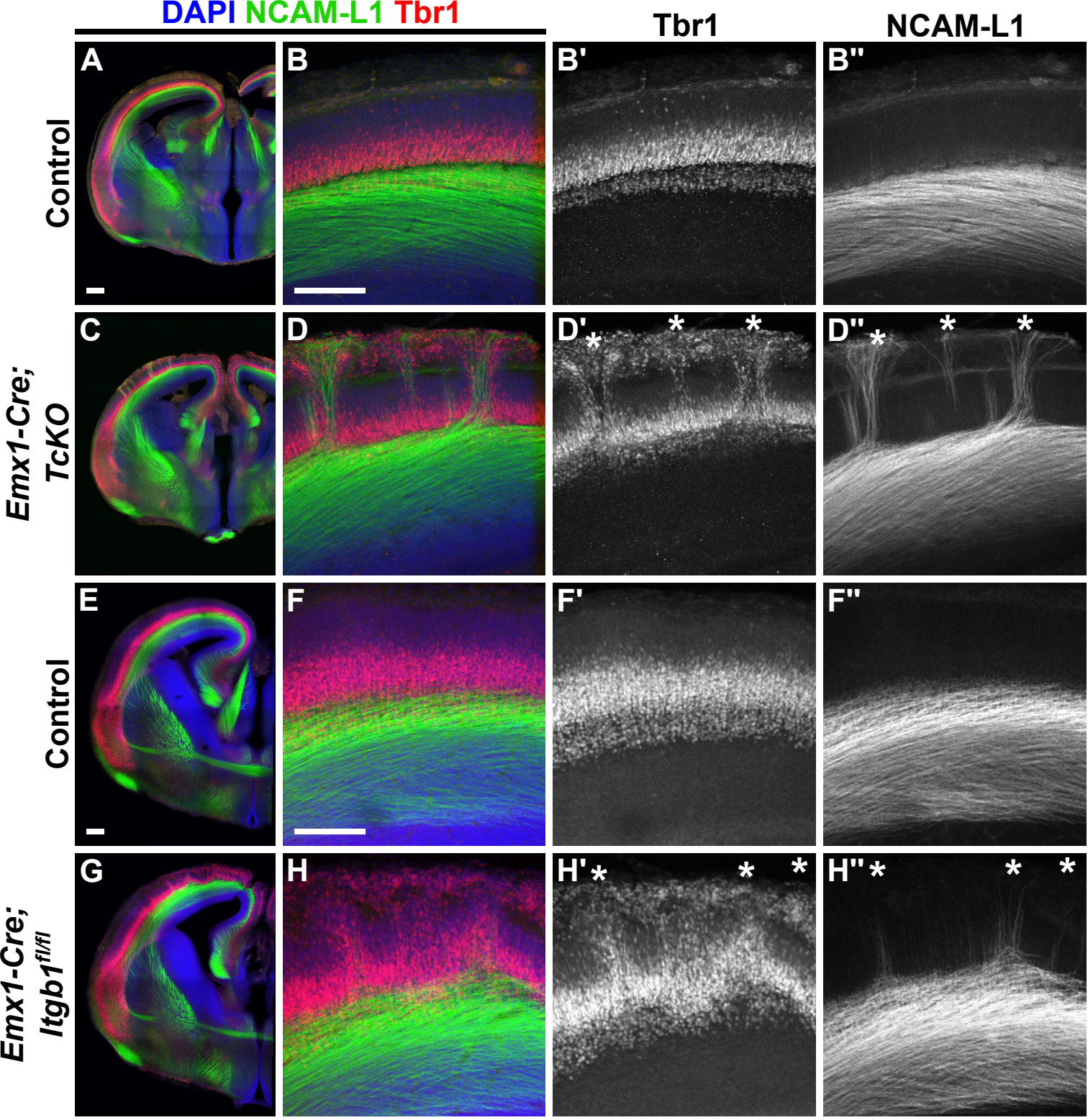
DAPI NCAM-L1 Tbr1
Tbr1
NCAM-L1
Control
Emx1-Cre; TcKO
Control
Emx1-Cre; Itgb1fl/fl
A
B
B'
B''
C
D
D'
D''
E
F
F'
F''
G
H
H'
H''

Figure 7

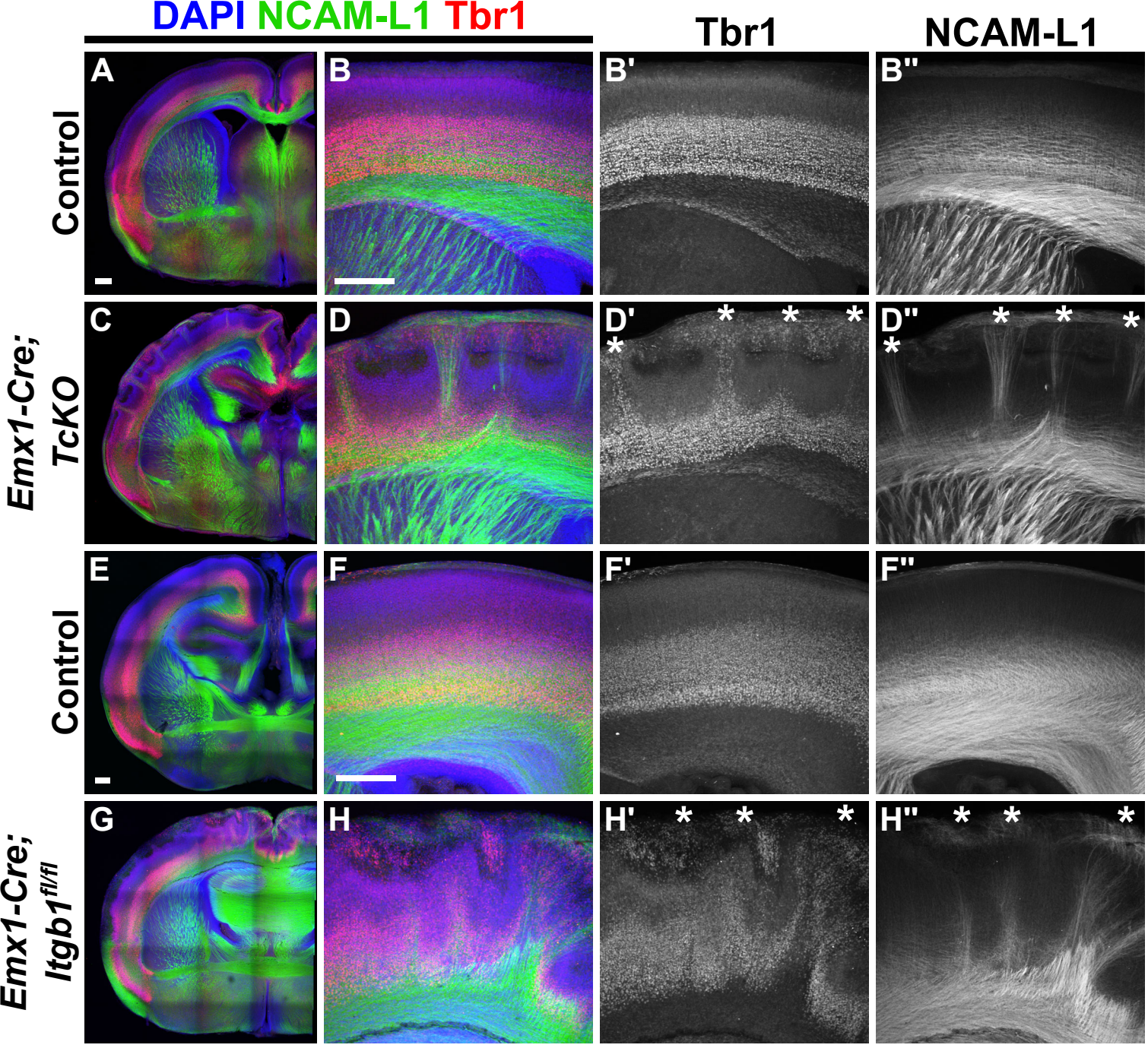
DAPI NCAM-L1 Tbr1
Tbr1
NCAM-L1
Control
Emx1-Cre; TcKO
Control
Emx1-Cre; Itgb1fl/fl
A
B
B'
B''
C
D
D'
D''
E
F
F'
F''
G
H
H'
H''

Figure 8